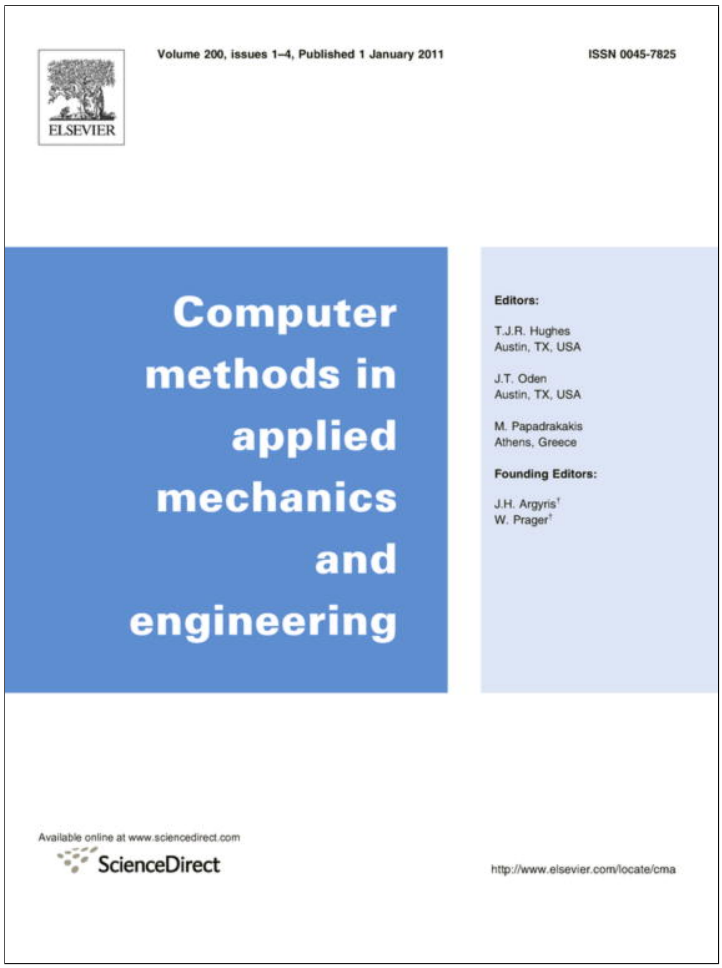

(This is a sample cover image for this issue. The actual cover is not yet available at this time.)

Comput. Methods Appl. Mech. Engrg. 200 (2011) 1804–1821

Contents lists available at ScienceDirect

Comput. Methods Appl. Mech. Engrg.

journal homepage: www.elsevier.com/locate/cma

A reduced spectral function approach for the stochastic finite element analysis

S. Adhikari *

College of Engineering, Swansea University, Singleton Park, Swansea SA2 8PP, UK

ARTICLE INFO

Article history:
Received 25 June 2010
Received in revised form 14 January 2011
Accepted 17 January 2011
Available online 3 February 2011

Keywords:
Stochastic PDE
Random field
Spectral decomposition
Karhunen–Loève expansion
Orthonormal basis

ABSTRACT

The stochastic finite element analysis of elliptic type partial differential equations with non-Gaussian random fields are considered. A novel approach by projecting the solution of the discretized equation into a reduced finite dimensional orthonormal vector basis is investigated. It is shown that the solution can be obtained using a finite series comprising functions of random variables and orthonormal vectors. These functions, called as the spectral functions, can be expressed in terms of the spectral properties of the deterministic coefficient matrices arising due to the discretization of the governing partial differential equation. Based on the projection in a reduced orthonormal vector basis, a Galerkin error minimization approach is proposed. The constants appearing in the Galerkin method are solved from a system of linear equations which has much smaller dimension compared to the original discretized equation. A hybrid analytical and simulation based computational approach is proposed to obtain the moments and probability density function of the solution. The method is illustrated using the stochastic nanomechanics of a zinc oxide (ZnO) nanowire deflected under the atomic force microscope (AFM) tip. The results are compared with the results obtained using direct Monte Carlo simulation, classical Neumann expansion and polynomial chaos approach for different correlation lengths and strengths of randomness.

1. Introduction

Due to the significant development in computational hardware it is now possible to solve very high resolution models in various computational physics problems, ranging from fluid mechanics to nano-bio mechanics. However, the spatial resolution is not enough to determine the credibility of a numerical model. The physical model as well its parameters are also crucial. Since neither of these may not be exactly known, over the past three decades there has been increasing research activities to model the governing partial differential equations within the framework of stochastic equations. We refer to few recent review papers [1–3]. Consider a bounded domain $\mathcal{D} \in \mathbb{R}^d$ with piecewise Lipschitz boundary $\partial\mathcal{D}$, where $d \leqslant 3$ is the spatial dimension. Further, consider that $(\Omega, \mathcal{F}, P)$ is a probability space where $\omega \in \Omega$ is a sample point from the sampling space Ω, $\mathcal{F}$ is the complete σ-algebra over the subsets of Ω and P is the probability measure. We consider the stochastic elliptic partial differential equation (PDE)

$$-\nabla[a(\mathbf{r},\omega)\nabla u(\mathbf{r},\omega)] = p(\mathbf{r}); \quad \mathbf{r} \quad \text{in } \mathcal{D} \tag{1}$$

with the associated Dirichlet condition

$$u(\mathbf{r},\omega) = 0; \quad \mathbf{r} \quad \text{on } \partial\mathcal{D}. \tag{2}$$

Here $a : \mathbb{R}^d \times \Omega \to \mathbb{R}$ is a random field [4], which can be viewed as a set of random variables indexed by $\mathbf{r} \in \mathbb{R}^d$. We assume the random field $a(\mathbf{r},\omega)$ to be stationary and square integrable. Depending on the physical problem the random field $a(\mathbf{r},\omega)$ can be used to model different physical quantities. As an example, for a slow flow of an incompressible, viscous fluid through a porus media, $a(\mathbf{r},\omega)$ would be the random field describing the permeability of the medium. The purpose of this paper is to investigate a new solution approach for Eq. (1) after the discretization using the stochastic finite element method. The stochastic finite element method (SFEM) is now a well established technique and the readers are refereed to earlier works which cover the basics [5–7].

In Section 2 a brief overview of spectral stochastic finite element method is presented. The projection theory in the vector space is developed in Section 3. In Section 4 an error minimization approach in the Hilbert space is proposed. The idea of the reduced orthonormal vector basis is introduced in Section 5. The post processing of the results to obtain the response moments are discussed in Section 6. Based on the theocratical results, a simple computational approach is proposed in sub Section 6.2. The numerical approach is applied to the stochastic mechanics of zinc oxide (ZnO) nanowires in Section 7. From the theoretical developments and numerical results, some conclusions are drawn in Section 8.

* Tel.: +44 01792 602088; fax: +44 01792 295676.
E-mail address: S.Adhikari@swansea.ac.uk

0045-7825/$ - see front matter © 2011 Elsevier B.V. All rights reserved.
doi:10.1016/j.cma.2011.01.015

2. Overview of the spectral stochastic finite element method

2.1. Discretization of the stochastic PDE

First consider $a(\mathbf{r},\omega)$ is a Gaussian random field with a covariance function $C_a : \mathbb{R}^d \times \mathbb{R}^d \to \mathbb{R}$ defined in the domain $\mathcal{D}$. Since the covariance function is square bounded, symmetric and positive definite, it can be represented by a spectral decomposition in an infinite dimensional Hilbert space. Using this spectral decomposition, the random process $a(\mathbf{r},\omega)$ can be expressed [5,8, see for example] in a generalized Fourier type of series known as the Karhunen–Loève (KL) expansion

$$a(\mathbf{r},\omega) = a_0(\mathbf{r}) + \sum_{i=1}^{\infty} \sqrt{v_i}\,\widetilde{\xi}_i(\omega)\varphi_i(\mathbf{r}). \tag{3}$$

Here $a_0(\mathbf{r})$ is the mean function, $\widetilde{\xi}_i(\omega)$ are uncorrelated standard Gaussian random variables, v_i and $\varphi_i(\mathbf{r})$ are eigenvalues and eigenfunctions satisfying the integral equation

$$\int_{\mathcal{D}} C_a(\mathbf{r}_1,\mathbf{r}_2)\varphi_j(\mathbf{r}_1)\mathrm{d}\mathbf{r}_1 = v_j\varphi_j(\mathbf{r}_2) \quad \forall\, j = 1,2,\ldots \tag{4}$$

The Gaussian random field model is not applicable for strictly positive quantities arising in many practical problems. Eq. (3) could also represent the Karhunen–Loève expansion of a non-Gaussian random field, which is also well defined. Alternatively, when $a(\mathbf{r},\omega)$ is a general non-Gaussian random field, it can be expressed in a mean-square convergent series in random variables and spatial functions using the polynomial chaos expansion. For example Ghanem [9] expanded log-normal random fields in a polynomial chaos expansion. In general, non Gaussian random fields can be expressed in a series like

$$a(\mathbf{r},\omega) = a_0(\mathbf{r}) + \sum_{i=1}^{\infty} \xi_i(\omega)a_i(\mathbf{r}), \tag{5}$$

using Wiener–Askey chaos expansion [10–12]. Here $\xi_i(\omega)$ are in general non-Gaussian and correlated random variables and $a_i(\mathbf{r})$ are deterministic functions. In this paper we use this general form of the decomposition of the random field.

Truncating the series (5) up to the Mth term, substituting $a(\mathbf{r},\omega)$ in the governing PDE (1) and applying the boundary conditions, the discretized equation can be written as

$$\left[\mathbf{A}_0 + \sum_{i=1}^{M} \xi_i(\omega)\mathbf{A}_i\right]\mathbf{u}(\omega) = \mathbf{f}. \tag{6}$$

Here the global matrices can be expressed as

$$\mathbf{A}_i = \sum_e \mathbf{A}_i^{(e)}; \quad i = 0,1,2,\ldots,M. \tag{7}$$

The element matrices $\mathbf{A}_i^{(e)}$ are defined over an element domain $\mathcal{D}_e \in \mathcal{D}$ such that $\mathcal{D}_e \bigcap \mathcal{D}_{e'} = \emptyset$ for $e \neq e'$ and $\bigcup_{\forall e}\mathcal{D}_e = \mathcal{D}$ and can be given by

$$\mathbf{A}_0^{(e)} = \int_{\mathcal{D}_e} \mathrm{d}\mathbf{r}\, a_0(\mathbf{r})\mathbf{B}^{(e)^T}(\mathbf{r})\mathbf{B}^{(e)}(\mathbf{r}) \tag{8}$$

$$\text{and} \quad \mathbf{A}_i^{(e)} = \sqrt{v_i}\int_{\mathcal{D}_e} \mathrm{d}\mathbf{r}\, a_i(\mathbf{r})\mathbf{B}^{(e)^T}(\mathbf{r})\mathbf{B}^{(e)}(\mathbf{r}); \quad i = 1,2,\ldots,M \tag{9}$$

In the above equations the $\mathbf{B}^{(e)}(\mathbf{r})$ is a deterministic matrix related to the shape function used to interpolate the solution within the element e. For the elliptic problem it can be shown [13] that $\mathbf{B}^{(e)}(\mathbf{r}) = \nabla\mathbf{N}^{(e)}(\mathbf{r})$. The necessary technical details to obtain the discrete stochastic algebraic equations from the stochastic partial differential Eq. (1) have become standard in the literature. Excellent references, for example [5,14–16] are available on this topic. In Eq. (6), $\mathbf{A}_0$ is a symmetric positive definite matrix, $\mathbf{A}_i \in \mathbb{R}^{n\times n}$; $i = 1,2,\ldots,M$ are symmetric matrices, $\mathbf{u}(\omega) \in \mathbb{R}^n$ is the solution vector and $\mathbf{f} \in \mathbb{R}^n$ in the input vector. We assume that the eigenvalues of $\mathbf{A}_0$ are distinct. For most practical application uncertainties are small compared to the deterministic values. Therefore, we normally have

$$\|\mathbf{A}_0\| \geqslant \|\sum_{i=1}^{M} \xi_i(\omega)\mathbf{A}_i\|; \quad \forall\ \omega \in \Omega. \tag{10}$$

Here by $\|\bullet\|$ we imply the Frobenius matrix norm [17], defined as $\|\mathbf{A}\| = \mathrm{Trace}\,(\mathbf{A}\mathbf{A}^T)$ for any $\mathbf{A} \in \mathbb{R}^{n\times n}$. The number of terms M in Eq. (6) can be selected based on the accuracy desired for the representation of the underlying random field. One of the main aim of a stochastic finite element analysis is to obtain $\mathbf{u}(\omega)$ for $\omega \in \Omega$ from Eq. (6) in an efficient manner and is the main topic of this paper. We propose a solution technique for Eq. (6) when $\xi_i(\omega)$ are in general non-Gaussian and correlated random variables.

2.2. Brief review of the solution techniques

The solution of the set of stochastic linear algebraic equations (6) is a key step in the stochastic finite element analysis. As a result, several methods have been proposed. These methods include, first- and second-order perturbation methods [6,18], Neumann expansion method [19,20], Galerkin approach [21], linear algebra based methods [22–24] and simulation methods [25]. More recently efficient collocation methods have been proposed [26,27]. Another class of methods which have been used widely in the literature is known as the spectral methods (see [1] for a recent review). These methods include the polynomial chaos (PC) expansion [5], stochastic reduced basis method [28–30] and Wiener–Askey chaos expansion [10–12]. According to the polynomial chaos expansion, second-order random variables $u_j(\theta)$ can be represented by the mean-square convergent expansion

$$\begin{aligned} u_j(\omega) = {} & u_{i_0}h_0 + \sum_{i_1=1}^{\infty} u_{i_1}h_1(\xi_{i_1}(\omega)) + \sum_{i_1=1}^{\infty}\sum_{i_2=1}^{i_1} u_{i_1,i_2}h_2(\xi_{i_1}(\omega),\xi_{i_2}(\omega)) \\ & + \sum_{i_1=1}^{\infty}\sum_{i_2=1}^{i_1}\sum_{i_3=1}^{i_2} u_{i_1i_2i_3}h_3(\xi_{i_1}(\omega),\xi_{i_2}(\omega),\xi_{i_3}(\omega)) \\ & + \sum_{i_1=1}^{\infty}\sum_{i_2=1}^{i_1}\sum_{i_3=1}^{i_2}\sum_{i_4=1}^{i_3} u_{i_1i_2i_3i_4}h_4(\xi_{i_1}(\omega),\xi_{i_2}(\omega),\xi_{i_3}(\omega),\xi_{i_4}(\omega)) + \cdots, \end{aligned} \tag{11}$$

where $u_{i_1,\ldots,i_r}$ are deterministic constants to be determined and $h_r\xi_{i_1}(\omega),\ldots,\xi_{i_r}(\omega)$ is the rth order homogeneous Chaos. When $\xi_i(\omega)$ are Gaussian random variables, the functions $h_r(\xi_{i_1}(\omega),\ldots,\xi_{i_r}(\omega))$ are the rth order Hermite polynomial so that it becomes orthonormal with respect to the Gaussian probability density function. The same idea can be extended to non-Gaussian random variables, provided more generalized functional basis are used [10–12] so that the orthonormality with respect to the probability density functions can be retained. When we have a random vector, as in the case of the solution of Eq. (6), then it is natural to replace the constants $u_{i_1,\ldots,i_r}$ by vectors $\mathbf{u}_{i_1,\ldots,i_r} \in \mathbb{R}^n$. Suppose the series is truncated after P number of terms. The value of P depends on the number of basic random variables M and the order of the PC expansion r as

$$P = \sum_{j=0}^{r} \frac{(M+j-1)!}{j!(M-1)!} = \binom{M+r}{r}. \tag{12}$$

After the truncation, there are P number of unknown vectors of dimension n. Then a mean-square error minimization approach can be applied and the unknown vectors can be solved using the Galerkin approach [5]. Since P increases very rapidly with the order of the chaos r and the number of random variables M, the final

number of unknown constants Pn becomes very large. As a result several methods have been developed (see for example [28–32]) to reduce the computational cost. In the polynomial chaos based solution approach, the *only* information used to construct the basis is the probability density function of the random variables. In the context of the discretized Eq. (6), more information such as the matrices $\mathbf{A}_i$, $i = 0, 1, 2, \ldots, M$ are available. It may be possible to construct alternative basis using these matrices. Here we investigate such an approach, where instead of projecting the solution in the space of orthonormal polynomials, the solution is projected in an orthonormal vector basis generated from the coefficient matrices.

3. Spectral decomposition in the vector space

3.1. Derivation of the spectral functions

Following the spectral stochastic finite element method, or otherwise, an approximation to the solution of Eq. (6) can be expressed as a linear combination of functions of random variables and deterministic vectors. Recently Nouy [33,34] discussed the possibility of an optimal spectral decomposition. The aim is to use small number of terms to reduce the computation without loosing the accuracy. Here an orthonormal vector basis is considered. Fixing a value of ω, say $\omega = \omega_1$, the solution of Eq. (6) $\mathbf{u}(\omega_1)$ can be expanded in a complete basis as $\mathbf{u}(\omega_1) = \alpha_1^{(1)}\boldsymbol{\phi}_1 + \alpha_2^{(1)}\boldsymbol{\phi}_2 + \cdots \alpha_n^{(1)}\boldsymbol{\phi}_n$. Repeating this for ω_1, $\omega_2, \ldots$ eventually the whole sample-space can be covered and it would be possible to expand $\mathbf{u}(\omega)$, $\forall\ \omega \in \Omega$ as a linear combination of $\boldsymbol{\phi}_1, \boldsymbol{\phi}_2, \ldots, \boldsymbol{\phi}_n$.

We use the eigenvectors $\boldsymbol{\phi}_k \in \mathbb{R}^n$ of the matrix $\mathbf{A}_0$ such that

$$\mathbf{A}_0\boldsymbol{\phi}_k = \lambda_{0_k}\boldsymbol{\phi}_k; \quad k = 1, 2, \ldots n \tag{13}$$

Since the matrix $\mathbf{A}_0$ is symmetric and generally positive definite, the eigenvectors $\boldsymbol{\phi}_k$ for $k = 1, 2, \ldots, n$ forms an orthonormal basis. Note that in principle any orthonormal basis can be used. This choice is selected due to the analytical simplicity as will be seen later. For notational convenience, define the matrix of eigenvalues and eigenvectors

$$\boldsymbol{\Lambda}_0 = \mathrm{diag}[\lambda_{0_1}, \lambda_{0_2}, \ldots, \lambda_{0_n}] \in \mathbb{R}^{n\times n} \quad \text{and} \quad \boldsymbol{\Phi} = [\boldsymbol{\phi}_1, \boldsymbol{\phi}_2, \ldots, \boldsymbol{\phi}_n] \in \mathbb{R}^{n\times n}. \tag{14}$$

Eigenvalues are ordered in the ascending order so that $\lambda_{0_1} < \lambda_{0_2} < \cdots < \lambda_{0_n}$. Since $\boldsymbol{\Phi}$ is an orthonormal matrix we have $\boldsymbol{\Phi}^{-1} = \boldsymbol{\Phi}^T$ so that the following identities can be easily established:

$$\boldsymbol{\Phi}^T\mathbf{A}_0\boldsymbol{\Phi} = \boldsymbol{\Lambda}_0; \quad \mathbf{A}_0 = \boldsymbol{\Phi}^{-T}\boldsymbol{\Lambda}_0\boldsymbol{\Phi}^{-1} \quad \text{and} \quad \mathbf{A}_0^{-1} = \boldsymbol{\Phi}\boldsymbol{\Lambda}_0^{-1}\boldsymbol{\Phi}^T. \tag{15}$$

We also introduce the transformations

$$\widetilde{\mathbf{A}}_i = \boldsymbol{\Phi}^T\mathbf{A}_i\boldsymbol{\Phi} \in \mathbb{R}^{n\times n}; \quad i = 0, 1, 2, \ldots, M. \tag{16}$$

Note that $\widetilde{\mathbf{A}}_0 = \boldsymbol{\Lambda}_0$, a diagonal matrix and

$$\mathbf{A}_i = \boldsymbol{\Phi}^{-T}\widetilde{\mathbf{A}}_i\boldsymbol{\Phi}^{-1} \in \mathbb{R}^{n\times n}; \quad i = 1, 2, \ldots, M. \tag{17}$$

Suppose the solution of Eq. (6) is given by

$$\hat{\mathbf{u}}(\omega) = \left[\mathbf{A}_0 + \sum_{i=1}^{M}\xi_i(\omega)\mathbf{A}_i\right]^{-1}\mathbf{f}. \tag{18}$$

Using Eqs. (14)–(17) and the orthonormality of $\boldsymbol{\Phi}$ one has

$$\hat{\mathbf{u}}(\omega) = \left[\boldsymbol{\Phi}^{-T}\boldsymbol{\Lambda}_0\boldsymbol{\Phi}^{-1} + \sum_{i=1}^{M}\xi_i(\omega)\boldsymbol{\Phi}^{-T}\widetilde{\mathbf{A}}_i\boldsymbol{\Phi}^{-1}\right]^{-1}\mathbf{f} = \boldsymbol{\Phi}\boldsymbol{\Psi}(\xi(\omega))\boldsymbol{\Phi}^T\mathbf{f}, \tag{19}$$

where

$$\boldsymbol{\Psi}(\xi(\omega)) = \left[\boldsymbol{\Lambda}_0 + \sum_{i=1}^{M}\xi_i(\omega)\widetilde{\mathbf{A}}_i\right]^{-1} \tag{20}$$

and the M-dimensional random vector

$$\xi(\omega) = \{\xi_1(\omega), \xi_2(\omega), \ldots, \xi_M(\omega)\}^T. \tag{21}$$

Now we separate the diagonal and off-diagonal terms of the $\widetilde{\mathbf{A}}_i$ matrices as

$$\widetilde{\mathbf{A}}_i = \boldsymbol{\Lambda}_i + \boldsymbol{\Delta}_i, \quad i = 1, 2, \ldots, M. \tag{22}$$

Here the diagonal matrix

$$\boldsymbol{\Lambda}_i = \mathrm{diag}[\widetilde{\mathbf{A}}] = \mathrm{diag}[\lambda_{i_1}, \lambda_{i_2}, \ldots, \lambda_{i_n}] \in \mathbb{R}^{n\times n} \tag{23}$$

and the matrix containing only the off-diagonal elements $\boldsymbol{\Delta}_i = \widetilde{\mathbf{A}}_i - \boldsymbol{\Lambda}_i$ is such that Trace $(\boldsymbol{\Delta}_i) = 0$. Using these, from Eq. (20) one has

$$\boldsymbol{\Psi}(\xi(\omega)) = \left[\underbrace{\boldsymbol{\Lambda}_0 + \sum_{i=1}^{M}\xi_i(\omega)\boldsymbol{\Lambda}_i}_{\boldsymbol{\Lambda}(\xi(\omega))} + \underbrace{\sum_{i=1}^{M}\xi_i(\omega)\boldsymbol{\Delta}_i}_{\boldsymbol{\Delta}(\xi(\omega))}\right]^{-1}, \tag{24}$$

where $\boldsymbol{\Lambda}(\xi(\omega)) \in \mathbb{R}^{n\times n}$ is a diagonal matrix and $\boldsymbol{\Delta}(\xi(\omega))$ is an off-diagonal only matrix. We rewrite Eq. (24) as

$$\boldsymbol{\Psi}(\xi(\omega)) = \left[\boldsymbol{\Lambda}(\xi(\omega))\left[\mathbf{I}_n + \boldsymbol{\Lambda}^{-1}(\xi(\omega))\boldsymbol{\Delta}(\xi(\omega))\right]\right]^{-1}. \tag{25}$$

The above expression can be represented using a Neumann type of matrix series [19] as

$$\boldsymbol{\Psi}(\xi(\omega)) = \sum_{s=0}^{\infty}(-1)^s\left[\boldsymbol{\Lambda}^{-1}(\xi(\omega))\boldsymbol{\Delta}(\xi(\omega))\right]^s\boldsymbol{\Lambda}^{-1}(\xi(\omega)). \tag{26}$$

Taking an arbitrary rth element of $\hat{\mathbf{u}}(\omega)$, Eq. (19) can be rearranged to have

$$\hat{u}_r(\omega) = \sum_{k=1}^{n}\Phi_{rk}\left(\sum_{j=1}^{n}\Psi_{kj}(\xi(\omega))\left(\boldsymbol{\phi}_j^T\mathbf{f}\right)\right). \tag{27}$$

Defining

$$\Gamma_k(\xi(\omega)) = \sum_{j=1}^{n}\Psi_{kj}(\xi(\omega))(\boldsymbol{\phi}_j^T\mathbf{f}) \tag{28}$$

and collecting all the elements in Eq. (27) for $r = 1, 2, \ldots, n$ one has

$$\hat{\mathbf{u}}(\omega) = \sum_{k=1}^{n}\Gamma_k(\xi(\omega))\boldsymbol{\phi}_k. \tag{29}$$

This shows that the solution vector $\hat{\mathbf{u}}(\omega)$ can be projected in the space spanned by $\boldsymbol{\phi}_k$.

Now assume the series in Eq. (26) is truncated after mth term. We define the truncated function

$$\boldsymbol{\Psi}^{(m)}(\xi(\omega)) = \sum_{s=0}^{m}(-1)^s\left[\boldsymbol{\Lambda}^{-1}(\xi(\omega))\boldsymbol{\Delta}(\xi(\omega))\right]^s\boldsymbol{\Lambda}^{-1}(\xi(\omega)). \tag{30}$$

From this one can obtain a sequence for different m

$$\hat{\mathbf{u}}^{(m)}(\omega) = \sum_{k=1}^{n}\Gamma_k^{(m)}(\xi(\omega))\boldsymbol{\phi}_k; \quad m = 1, 2, 3, \ldots \tag{31}$$

Since $\omega \in \Omega$ is arbitrary, comparing (6) and (18) we observe that $\hat{\mathbf{u}}^{(m)}(\omega)$ is the solution of Eq. (6) for every ω when $m \to \infty$. This implies that

$$\mathrm{Prob}\left\{\omega \in \Omega : \lim_{m\to\infty}\hat{\mathbf{u}}^{(m)}(\omega) = \hat{\mathbf{u}}(\omega)\right\} = 1. \tag{32}$$

Therefore, $\hat{\mathbf{u}}(\omega)$ is the solution of Eq. (6) in probability. In this derivation, the probability density function of the random variables has not been used. Therefore, the random variables can be general as long as the solution exists.

Remark 1. The matrix power series in (26) is different from the classical Neumann series [19]. The classical Neumann series is a power series in $\mathbf{A}_0^{-1}[\Delta\mathbf{A}(\xi(\omega))]$, where the first term is deterministic and the second term is random. The elements of this matrix series are polynomials in $\xi_i(\omega)$. In contrast, the series in (26) is in terms of $[\mathbf{\Lambda}^{-1}\ (\xi(\omega))][\mathbf{\Delta}(\xi(\omega))]$, where both terms are random. The elements of this matrix series are not simple polynomials in $\xi_i(\omega)$, but are in terms of a ratio of polynomials as seen in Eq. (34). The convergence of this series depends of the spectral radius of

$$\mathbf{R} = \mathbf{\Lambda}^{-1}(\xi(\omega))\mathbf{\Delta}(\xi(\omega)). \tag{33}$$

A generic term of this matrix can be obtained as

$$R_{rs} = \frac{\Delta_{rs}}{\Lambda_{rr}} = \frac{\sum_{i=1}^{M}\xi_i(\omega)\Delta_{i_{rs}}}{\lambda_{0_r}+\sum_{i=1}^{M}\xi_i(\omega)\lambda_{i_r}} = \frac{\sum_{i=1}^{M}\xi_i(\omega)\widetilde{A}_{i_{rs}}}{\lambda_{0_r}+\sum_{i=1}^{M}\xi_i(\omega)\widetilde{A}_{i_{rr}}}; \quad r \neq s. \tag{34}$$

Since $\mathbf{A}_0$ is positive definite, $\lambda_{0_r} > 0$ for all r. It can be seen from Eq. (34) that the spectral radius of $\mathbf{R}$ is also controlled by the diagonal dominance of the $\widetilde{\mathbf{A}}_i$ matrices. If the diagonal terms are relatively larger than the off-diagonal terms, the series will converge faster even if the relative magnitude of λ_{0_r} is not large.

The series in (31) approaches to the exact solution of the governing Eq. (6) for every $\omega \in \Omega$ for $m \to \infty$. For this reason it converges in probability 1. The convergence in probability 1 is a stronger convergence than, for example, the mean-square convergence often used in the stochastic finite element analysis. Since the convergence in probability 1 automatically implies the mean-square convergence, the series in Eq. (29) is also a mean-square convergent series.

Definition 1. The functions $\Gamma_k(\xi(\omega))$, $k = 1, 2, \ldots, n$ are called the spectral functions as they are expressed in terms of the spectral properties of the coefficient matrix $\mathbf{A}_0$ arising in the discretized equation.

For certain class of problems the series in Eq. (29) can give useful physical insights into the uncertainty propagation. For structural mechanics problems, the matrix $\mathbf{A}_0$ is the stiffness matrix and its eigenvectors $\boldsymbol{\phi}_k$ are proportional to vibrational modes with a lumped mass assumption [35]. Eq. (29) says that the response of a stochastic system is a linear combination of the fundamental deformation modes weighted by the random variables Γ_k.

3.2. Properties of the spectral functions

In this section we discuss some important properties of these functions. From the series expansion in Eq. (26) we have

$$\begin{aligned}\mathbf{\Psi}(\xi(\omega)) = {} & \mathbf{\Lambda}^{-1}(\xi(\omega)) - \mathbf{\Lambda}^{-1}(\xi(\omega))\mathbf{\Delta}(\xi(\omega))\mathbf{\Lambda}^{-1}(\xi(\omega)) \\ & + \mathbf{\Lambda}^{-1}(\xi(\omega))\mathbf{\Delta}(\xi(\omega))\mathbf{\Lambda}^{-1}(\xi(\omega))\mathbf{\Delta}(\xi(\omega))\mathbf{\Lambda}^{-1}(\xi(\omega)) + \cdots\end{aligned} \tag{35}$$

Since $\mathbf{\Lambda}(\xi(\omega))$ is a diagonal matrix, its inverse is simply a diagonal matrix containing the inverse of each of the diagonal elements. Also recall that the diagonal of $\mathbf{\Delta}(\xi(\omega))$ contains only zeros. Different terms of the series in (35) can be obtained using a simple recursive relationship [19]. The numerical computation of the series is therefore computationally very efficient. For further analytical results, the spectral functions of the different orders are defined by truncating the series up to different terms.

Definition 2. The first-order spectral functions $\Gamma_k^{(1)}(\boldsymbol{\xi}(\omega)), k = 1, 2, \ldots, n$ are obtained by retaining only one term in the series (35).

Retaining one term in (35) we have

$$\mathbf{\Psi}^{(1)}(\xi(\omega)) = \mathbf{\Lambda}^{-1}(\xi(\omega)) \quad \text{or} \quad \Psi_{kj}^{(1)}(\xi(\omega)) = \frac{\delta_{kj}}{\lambda_{0_k}+\sum_{i=1}^{M}\xi_i(\omega)\lambda_{i_k}}. \tag{36}$$

Using the definition of the spectral function in Eq. (28), the first-order spectral functions can be explicitly obtained as

$$\Gamma_k^{(1)}(\xi(\omega)) = \sum_{j=1}^{n}\Psi_{kj}^{(1)}(\xi(\omega))(\boldsymbol{\phi}_j^T\mathbf{f}) = \frac{\boldsymbol{\phi}_k^T\mathbf{f}}{\lambda_{0_k}+\sum_{i=1}^{M}\xi_i(\omega)\lambda_{i_k}}. \tag{37}$$

From this expression it is clear that $\Gamma_k^{(1)}(\xi(\omega))$ are correlated non-Gaussian random variables. Since we assumed that all eigenvalues λ_{0_k} are distinct, every $\Gamma_k^{(1)}(\xi(\omega))$ in Eq. (37) are different for different values of k.

Definition 3. The second-order spectral functions $\Gamma_k^{(2)}(\xi(\omega))$, $k = 1, 2, \ldots, n$ are obtained by retaining two terms in the series (35).

Retaining two terms in (35) we have

$$\mathbf{\Psi}^{(2)}(\xi(\omega)) = \mathbf{\Lambda}^{-1}(\xi(\omega)) - \mathbf{\Lambda}^{-1}(\xi(\omega))\mathbf{\Delta}(\xi(\omega))\mathbf{\Lambda}^{-1}(\xi(\omega)), \tag{38}$$

$$\begin{aligned}\text{or} \quad \Psi_{kj}^{(2)}(\xi(\omega)) = {} & \frac{\delta_{kj}}{\lambda_{0_k}+\sum_{i=1}^{M}\xi_i(\omega)\lambda_{i_k}} \\ & - \frac{\sum_{i=1}^{M}\xi_i(\omega)\Delta_{i_{kj}}}{\left(\lambda_{0_k}+\sum_{i=1}^{M}\xi_i(\omega)\lambda_{i_k}\right)\left(\lambda_{0_j}+\sum_{i=1}^{M}\xi_i(\omega)\lambda_{i_j}\right)}.\end{aligned} \tag{39}$$

Using the definition of the spectral function in Eq. (28), the second-order spectral functions can be obtained in closed-form as

$$\begin{aligned}\Gamma_k^{(2)}(\xi(\omega)) = {} & \frac{\boldsymbol{\phi}_k^T\mathbf{f}}{\lambda_{0_k}+\sum_{i=1}^{M}\xi_i(\omega)\lambda_{i_k}} \\ & - \sum_{\substack{j=1\\ j\neq k}}^{n}\frac{\left(\boldsymbol{\phi}_j^T\mathbf{f}\right)\sum_{i=1}^{M}\xi_i(\omega)\Delta_{i_{kj}}}{(\lambda_{0_k}+\sum_{i=1}^{M}\xi_i(\omega)\lambda_{i_k})(\lambda_{0_j}+\sum_{i=1}^{M}\xi_i(\omega)\lambda_{i_j})}.\end{aligned} \tag{40}$$

The second-order function can be viewed as adding corrections to the first-order expression derived in Eq. (37).

Definition 4. The vector of spectral functions of order s can be obtained by retaining s terms in the series (35) and can be expressed as

$$\mathbf{\Gamma}^{(s)}(\xi(\omega)) = \left[\mathbf{I}_n - \mathbf{R}(\xi(\omega)) + \mathbf{R}(\xi(\omega))^2 - \mathbf{R}(\xi(\omega))^3 \ldots s^{\text{thterm}}\right]\mathbf{\Gamma}^{(1)}(\xi(\omega)), \tag{41}$$

where $\mathbf{I}_n$ is the n-dimensional identity matrix and $\mathbf{R}$ is defined in Eq. (33) as $\mathbf{R}(\xi(\omega)) = [\mathbf{\Lambda}^{-1}(\xi(\omega))]\ [\mathbf{\Delta}(\xi(\omega))]$. Different terms of this series can be obtained recursively from the previous term [19].

In order to obtain further insight into these functions, we look into the functional nature of the solution $\mathbf{u}(\omega)$ in terms of the random variables $\xi_i(\omega)$. Suppose we denote

$$\mathbf{A}(\omega) = \left[\mathbf{A}_0 + \sum_{i=1}^{M}\xi_i(\omega)\mathbf{A}_i\right] \in \mathbb{R}^{n\times n}, \tag{42}$$

so that

$$\mathbf{u}(\omega) = \mathbf{A}^{-1}(\omega)\mathbf{f}. \tag{43}$$

From the definition of the matrix inverse (omitting ω for notational convenience) we have

$$\mathbf{A}^{-1} = \frac{\text{Adj}(\mathbf{A})}{\det(\mathbf{A})} = \frac{\mathbf{C}_a^T}{\det(\mathbf{A})}, \tag{44}$$

where $\mathbf{C}_a$ is the matrix of cofactors. The determinant of $\mathbf{A}$ contains a maximum of n number of products of A_{kj} and their linear combinations. Note from Eq. (42) that

$$A_{kj}(\omega) = A_{0_{kj}} + \sum_{i=1}^{M} \xi_i(\omega)\mathbf{A}_{i_{kj}}. \tag{45}$$

Since all the matrices are of full rank, the determinant contains a maximum of n number of products of linear combination of random variables in Eq. (45). On the other hand, each entries of the matrix of cofactors, contains a maximum of $(n-1)$ number of products of linear combination of random variables in Eq. (45). From Eqs. (43) and (44) it follows that:

$$\mathbf{u}(\omega) = \frac{\mathbf{C}_a^T\mathbf{f}}{\det(\mathbf{A})}. \tag{46}$$

Therefore, the numerator of each element of the solution vector contains linear combinations of the elements of the cofactor matrix, which are complete polynomials of order $(n-1)$. This implies that the elements of $\mathbf{u}(\omega)$ are the ratio of polynomials of the form

$$\frac{p^{(n-1)}(\xi_1(\omega),\xi_2(\omega),\ldots,\xi_M(\omega))}{p^{(n)}(\xi_1(\omega),\xi_2(\omega),\ldots,\xi_M(\omega))}, \tag{47}$$

where $p^{(n)}(\xi_1(\omega),\xi_2(\omega),\ldots,\xi_M(\omega))$ is an nth order complete multivariate polynomial of variables $\xi_1(\omega)$, $\xi_2(\omega),\ldots,\xi_M(\omega)$.

This result is important because different solution methods essentially aim to approximate the ratio of the polynomials given in Eq. (47). It is clear that the functional form of the elements of the solution vector is *not* a polynomial in the random variables. Aiming to express the ratio of two polynomials, where the denominator has higher degree compared to the numerator, by a series of polynomials (e.g., in polynomial chaos, Neumann expansion or perturbation methods) may require many terms. It can be shown that the linear combination of the spectral functions has the same functional form in $(\xi_1(\omega),\xi_2(\omega),\ \ldots,\xi_M(\omega))$ as the elements of the solution vector given in Eq. (47).

When first-order spectral functions (37) are considered, we have

$$\hat{u}_r^{(1)}(\omega) = \sum_{k=1}^{n} \Gamma_k^{(1)}(\boldsymbol{\xi}(\omega))\phi_{rk} = \sum_{k=1}^{n} \frac{\boldsymbol{\phi}_k^T\mathbf{f}}{\lambda_{0_k} + \sum_{i=1}^{M}\xi_i(\omega)\lambda_{i_k}}\phi_{rk}. \tag{48}$$

All $\left(\lambda_{0_k} + \sum_{i=1}^{M}\xi_i(\omega)\lambda_{i_k}\right)$ are different for different k because it is assumed that all eigenvalues λ_{0_k} are distinct. Carrying out the above summation one has n number of products of $\left(\lambda_{0_k} + \sum_{i=1}^{M}\xi_i(\omega)\lambda_{i_k}\right)$ in the denominator and n sums of $(n-1)$ number of products of $\left(\lambda_{0_k} + \sum_{i=1}^{M}\xi_i(\omega)\lambda_{i_k}\right)$ in the numerator, that is,

$$\hat{u}_r^{(1)}(\omega) = \frac{\sum_{k=1}^{n}(\boldsymbol{\phi}_k^T\mathbf{f})\phi_{rk}\prod_{\substack{j=1\\ j\neq k}}^{n-1}\left(\lambda_{0_j} + \sum_{i=1}^{M}\xi_i(\omega)\lambda_{i_j}\right)}{\prod_{k=1}^{n-1}\left(\lambda_{0_j} + \sum_{i=1}^{M}\xi_i(\omega)\lambda_{i_j}\right)}. \tag{49}$$

This has the same form as Eq. (47). For the second-order spectral functions (40)

$$\begin{aligned}\hat{u}_r^{(2)}(\omega) &= \sum_{k=1}^{n}\Gamma_k^{(2)}(\boldsymbol{\xi}(\omega))\phi_{rk}\\ &= \sum_{k=1}^{n}\left[\frac{\boldsymbol{\phi}_k^T\mathbf{f}}{\lambda_{0_k} + \sum_{i=1}^{M}\xi_i(\omega)\lambda_{i_k}}\right.\\ &\quad\left. - \sum_{\substack{j=1\\ j\neq k}}^{n}\frac{\left(\boldsymbol{\phi}_j^T\mathbf{f}\right)\sum_{i=1}^{M}\xi_i(\omega)\Delta_{i_{kj}}}{\left(\lambda_{0_k} + \sum_{i=1}^{M}\xi_i(\omega)\lambda_{i_k}\right)\left(\lambda_{0_j} + \sum_{i=1}^{M}\xi_i(\omega)\lambda_{i_j}\right)}\right]\phi_{rk}\\ &= \hat{u}_r^{(1)}(\omega) - \sum_{k=1}^{n}\sum_{\substack{j=1\\ j\neq k}}^{n}\frac{\left(\boldsymbol{\phi}_j^T\mathbf{f}\right)\sum_{i=1}^{M}\xi_i(\omega)\Delta_{i_{kj}}}{\left(\lambda_{0_k} + \sum_{i=1}^{M}\xi_i(\omega)\lambda_{i_k}\right)\left(\lambda_{0_j} + \sum_{i=1}^{M}\xi_i(\omega)\lambda_{i_j}\right)}\phi_{rk}.\end{aligned} \tag{50}$$

Carrying out the above summation we again see that this has the same form as Eq. (47).

This proves that the nature of the solution has the same mathematical form of the exact solution, that is, the ratio of two polynomials in $(\xi_1(\omega),\xi_2(\omega),\ldots,\xi_M(\omega))$ where the numerator has a lower order compared to the denominator. This is in contrast with other methods such as the perturbation methods, classical Neumann series or polynomial chaos expansions, which are in effect simple polynomials in $(\xi_1(\omega),\xi_2(\omega),\ldots,\xi_M(\omega))$ (i.e., no polynomials in the denominator). Next we propose a Galerkin approach to minimize the error arising due to the truncation of the spectral functions.

4. Error minimization using the Galerkin approach

In Section 3.1 we derived the spectral functions such that a projection in an orthonormal basis converges to the exact solution in probability 1. The spectral functions are expressed in terms of a convergent infinite series. First, second and higher order spectral functions obtained by truncating the infinite series have been derived. We have also showed that they have the same functional form as the exact solution of Eq. (6). This motivates us to use these functions as 'trial functions' to construct the solution. The idea is to minimize the error arising due to the truncation. A Galerkin approach is proposed where the error is made orthogonal to the spectral functions.

We express the solution vector by the series representation

$$\hat{\mathbf{u}}(\omega) = \sum_{k=1}^{n} c_k\widehat{\Gamma}_k(\boldsymbol{\xi}(\omega))\boldsymbol{\phi}_k. \tag{51}$$

Here the functions $\widehat{\Gamma}_k : \mathbb{R}^M \to \mathbb{R}$ are the spectral functions and the constants $c_k \in \mathbb{R}$ need to be obtained using the Galerkin approach. The functions $\widehat{\Gamma}_k(\boldsymbol{\xi}(\omega))$ can be the first-order (37), second-order (40) or any higher-order spectral functions (41) and $\boldsymbol{\phi}_k$ are the eigenvectors introduced earlier in Eq. (13). Substituting the expansion of $\hat{\mathbf{u}}(\omega)$ in the governing Eq. (6), the error vector can be obtained as

$$\boldsymbol{\varepsilon}(\omega) = \left(\sum_{i=0}^{M}\mathbf{A}_i\xi_i(\omega)\right)\left(\sum_{k=1}^{n}c_k\widehat{\Gamma}_k(\boldsymbol{\xi}(\omega))\boldsymbol{\phi}_k\right) - \mathbf{f} \in \mathbb{R}^n \tag{52}$$

where $\xi_0 = 1$ is used to simplify the first summation expression. The expression (51) is viewed as a projection where $\{\widehat{\Gamma}_k(\boldsymbol{\xi}(\omega))\boldsymbol{\phi}_k\} \in \mathbb{R}^n$ are the basis functions and c_k are the unknown constants to be determined. We wish to obtain the coefficients c_k using the Galerkin approach so that the error is made orthogonal to the basis functions, that is, mathematically

$$\begin{aligned}&\boldsymbol{\varepsilon}(\omega) \perp \left(\widehat{\Gamma}_j(\boldsymbol{\xi}(\omega))\boldsymbol{\phi}_j\right) \quad \text{or} \quad <\widehat{\Gamma}_j(\boldsymbol{\xi}(\omega))\boldsymbol{\phi}_j,\ \boldsymbol{\varepsilon}(\omega)>=0\\ &\forall\quad j = 1,2,\ldots,n.\end{aligned} \tag{53}$$

Here $<\mathbf{u}(\omega),\mathbf{v}(\omega)>=\int_\Omega P(\mathrm{d}\omega)\mathbf{u}^T(\omega)\mathbf{v}(\omega)$ is the inner product norm. Imposing this condition and using the expression of $\boldsymbol{\varepsilon}(\omega)$ from Eq. (52) one has

$$\mathrm{E}\left[\widehat{\Gamma}_j(\boldsymbol{\xi}(\omega))\boldsymbol{\phi}_j^T\left(\sum_{i=0}^{M}\mathbf{A}_i\xi_i(\omega)\right)\left(\sum_{k=1}^{n}c_k\widehat{\Gamma}_k(\boldsymbol{\xi}(\omega))\boldsymbol{\phi}_k\right) - \widehat{\Gamma}_j(\boldsymbol{\xi}(\omega))\boldsymbol{\phi}_j^T\mathbf{f}\right] = 0 \quad \forall\, j. \tag{54}$$

Interchanging the E[•] and summation operations, this can be simplified to

$$\sum_{k=1}^{n}\left(\sum_{i=0}^{M}(\boldsymbol{\phi}_j^T\mathbf{A}_i\boldsymbol{\phi}_k)\mathrm{E}\left[\xi_i(\omega)\widehat{\Gamma}_j(\boldsymbol{\xi}(\omega))\widehat{\Gamma}_k(\boldsymbol{\xi}(\omega))\right]\right)c_k = \mathrm{E}[\widehat{\Gamma}_j(\boldsymbol{\xi}(\omega))]\left(\boldsymbol{\phi}_j^T\mathbf{f}\right) \tag{55}$$

$$\text{or}\quad \sum_{k=1}^{n}\left(\sum_{i=0}^{M}\widetilde{A}_{i_{jk}}D_{ijk}\right)c_k = b_j. \tag{56}$$

Defining the vector $\mathbf{c} = \{c_1, c_2, \ldots, c_n\}^T$, these equations can be expressed in a matrix form as

$$\mathbf{S}\mathbf{c} = \mathbf{b} \tag{57}$$

with

$$S_{jk} = \sum_{i=0}^{M} \widetilde{A}_{i_{jk}} D_{ijk}; \quad \forall\, j,k = 1,2,\ldots,n, \tag{58}$$

where

$$\widetilde{A}_{i_{jk}} = \boldsymbol{\phi}_j^T \mathbf{A}_i \boldsymbol{\phi}_k, \tag{59}$$

$$D_{ijk} = \mathrm{E}\left[\xi_i(\omega)\widehat{\Gamma}_j(\boldsymbol{\xi}(\omega))\widehat{\Gamma}_k(\boldsymbol{\xi}(\omega))\right] \tag{60}$$

$$\text{and} \quad b_j = \mathrm{E}\left[\widehat{\Gamma}_j(\boldsymbol{\xi}(\omega))\right]\left(\boldsymbol{\phi}_j^T \mathbf{f}\right). \tag{61}$$

Higher order spectral functions can be used to improve the accuracy and convergence of the series (51). This will be demonstrated in the numerical examples later in the paper.

Remark 2. Comparison with the classical spectral SFEM: We compare this Galerkin approach with the classical spectral stochastic finite element approach for further insight. The number of equations to be solved for the unknown coefficients in Eq. (57) is n, the same dimension as the original governing Eq. (6). There are only n unknown constants, as opposed to nP unknown constants arising in the polynomial chaos expansion. The coefficient matrix $\mathbf{S}$ and the vector $\mathbf{b}$ in Eq. (57) should be obtained numerically using the Monte Carlo simulation or other numerical integration technique. In the classical PC expansion, however, the coefficient matrix and the associated vector are obtained exactly in closed-form. In addition, the coefficient matrix is a sparse matrix whereas the matrix $\mathbf{S}$ in Eq. (57) is in general a fully populated matrix.

The series in Eq. (51) can also be viewed as an enhanced Neumann expansion method where the approximating functions have been generated using a Neumann type expansion. This aspect is numerically investigated later in details in Section 7.2. It can be observed that the matrix $\mathbf{S}$ in Eq. (57) is symmetric. Therefore, one need to determine $n(n+1)/2$ number of coefficients by numerical methods. Any numerical integration method, such as the Gaussian quadrature method, can be used to obtain the elements of D_{ijk} and b_j in Eq. (61). In this paper Monte Carlo simulation is used. The samples of the spectral functions $\widehat{\Gamma}_k(\boldsymbol{\xi}(\omega))$ can be simulated from Eqs. (37) and (40) or (41) depending on the order. These can be used to compute D_{ijk} and b_j from Eq. (61). The simulated spectral functions can also be 'recycled' to obtain the statistics and probability density function (pdf) of the solution. In summary, compared to the classical spectral stochastic finite element method, the proposed Galerkin approach results in a smaller size matrix but requires numerical integration techniques to obtain its entries. The numerical method proposed here therefore can be considered as a hybrid analytical-simulation approach.

5. Model reduction using a reduced number of basis

The Galerkin approach proposed in the previous section requires the solution of $n \times n$ algebraic equations. Although in general this is smaller compared to the polynomial chaos approach, the computational cost can still be high for large n as the coefficient matrix is in general a dense matrix. The aim of this section is to reduce it further so that, in addition to large number of random variables, problems with large degrees of freedom can also be solved efficiently.

Suppose the eigenvalues of $\mathbf{A}_0$ are arranged in an increasing order such that

$$\lambda_{0_1} < \lambda_{0_2} < \cdots < \lambda_{0_n}. \tag{62}$$

From the expression of the spectral functions observe that the eigenvalues appear in the denominator:

$$\Gamma_k^{(1)}(\boldsymbol{\xi}(\omega)) = \frac{\boldsymbol{\phi}_k^T \mathbf{f}}{\lambda_{0_k} + \sum_{i=1}^{M} \xi_i(\omega)\lambda_{i_k}}. \tag{63}$$

The numerator $(\boldsymbol{\phi}_k^T \mathbf{f})$ is the projection of the force on the deformation mode. Since the eigenvalues are arranged in an ascending order, the denominator of $|\Gamma_{k+r}^{(1)}(\boldsymbol{\xi}(\omega))|$ is larger than the denominator of $|\Gamma_k^{(1)}(\boldsymbol{\xi}(\omega))|$ according a suitable measure. The numerator $(\boldsymbol{\phi}_k^T \mathbf{f})$ depends on the nature of forcing and the eigenvectors. Although this quantity is deterministic, in general an ordering cannot be easily established for different values of k. Because all the eigenvectors are normalized to unity, it is reasonable to consider that $(\boldsymbol{\phi}_k^T \mathbf{f})$ does not vary significantly for different values of k. Using the ordering of the eigenvalues, one can select a small number ϵ such that $\lambda_{0_1}/\lambda_{0_p} < \epsilon$ for some value of p. Based on this, we can approximate the solution using a truncated series as

$$\hat{\mathbf{u}}(\omega) \approx \sum_{k=1}^{p} c_k \widehat{\Gamma}_k(\boldsymbol{\xi}(\omega))\boldsymbol{\phi}_k, \tag{64}$$

where c_k, $\widehat{\Gamma}_k(\boldsymbol{\xi}(\omega))$ and $\boldsymbol{\phi}_k$ are obtained following the procedure described in the previous section by letting the indices j, k only up to p in Eqs. (58) and (61). The accuracy of the series (64) can be improved in two ways, namely, (a) by increasing the number of terms p, or (b) by increasing the order of the spectral functions $\widehat{\Gamma}_k(\boldsymbol{\xi}(\omega))$.

Model reduction techniques have been widely used within the scope of proper orthogonal decomposition (POD) method [36–38]. Here the eigenvalues of a symmetric positive definite matrix (the covariance matrix of a snapshot the system response) are used for model reduction. In spite of this similarity, the reduction method proposed here is different from a POD since it only considers the operator and not the solution itself. Reduction based on eigensolution is of classical nature in various areas of applied mathematics, engineering and physics and extensive studies exist on this topic. It should be noted that the truncation in series (64) introduces errors. A rigorous mathematical quantification of error arising due to this truncation is beyond the scope of this article. The ratio of the eigenvalues $\lambda_{0_1}/\lambda_{0_p}$ gives a good indication, but the projection of the force on the eigenvector $(\boldsymbol{\phi}_k^T \mathbf{f})$ is also of importance. Since this quantity is problem dependent, care should be taken while applying this reduction method.

Remark 3. The reduction of the original problem by a projection on the set of dominant eigenvectors of a part of the operator is rather classical in model reduction techniques. It relies on the strong hypothesis that the solution can be well represented on this set of vectors. The impact of this truncation on the solution or a quantity of interest is not estimated in the article. The truncation criteria is based on the spectral decay of a part of the operator but not on the solution itself. By introducing this reduction, some essential features of the solution may not be captured always. The proposed method will only capture the projection of the solution $\mathbf{u}$ on the reduced basis ϕ_k, $k = 1,2,\ldots,p$, which could be unadapted to the complete representation of $\mathbf{u}$.

6. Post processing and computational approach

6.1. Moments of the solution

For the practical application of the method developed here, the efficient computation of the response moments and pdf is of crucial importance. A simulation based algorithm is proposed in this section. The coefficients c_k in Eq. (64) can be calculated from a

reduced set of equations given by (57). The reduced equations can be obtained by letting the indices j, k up to $p < n$ in Eqs. (58) and (61). After obtaining the coefficient vector $\mathbf{c} \in \mathbb{R}^p$, the statistical moments of the solution can be obtained from Eq. (64) using the Monte Carlo simulation. The spectral functions used to obtain the vector $\mathbf{c}$ itself, can be reused to obtain the statistics and pdf of the solution. The mean vector can be obtained as

$$\bar{\mathbf{u}} = \mathrm{E}[\hat{\mathbf{u}}(\omega)] = \sum_{k=1}^{p} c_k \mathrm{E}[\widehat{\Gamma}_k(\xi(\omega))]\boldsymbol{\phi}_k. \tag{65}$$

The covariance of the solution vector can be expressed as

$$\boldsymbol{\Sigma}_u = \mathrm{E}\Big[(\hat{\mathbf{u}}(\omega) - \bar{\mathbf{u}})(\hat{\mathbf{u}}(\omega) - \bar{\mathbf{u}})^T\Big] = \sum_{k=1}^{p}\sum_{j=1}^{p} c_k c_j \Sigma_{\Gamma_{kj}} \boldsymbol{\phi}_k \boldsymbol{\phi}_j^T, \tag{66}$$

where the elements of the covariance matrix of the spectral functions are given by

$$\Sigma_{\Gamma_{kj}} = \mathrm{E}\Big[\Big(\widehat{\Gamma}_k(\xi(\omega)) - \mathrm{E}[\widehat{\Gamma}_k(\xi(\omega))]\Big)\Big(\widehat{\Gamma}_j(\xi(\omega)) - \mathrm{E}[\widehat{\Gamma}_j(\xi(\omega))]\Big)\Big]. \tag{67}$$

6.2. Summary of the computational approach

Based on the results derived in the paper, a hybrid reduced simulation-analytical approach is proposed. The method is applicable to elliptic problems with general non-Gaussian random fields. The computational procedure for the solution of the stochastic elliptic PDE (1) can be implemented as follows:

1. Obtain the system matrices $\mathbf{A}_i$, $i = 0,1,2,\ldots,M$ and the forcing vector $\mathbf{f}$ by discretizing the governing stochastic partial differential equation using the well established stochastic finite element methodologies.
2. Solve the eigenvalue problem associated with the mean matrix $\mathbf{A}_0$
$$A_0\boldsymbol{\Phi} = \boldsymbol{\Phi}\boldsymbol{\Lambda}_0. \tag{68}$$
3. Select a small value of ϵ, say $\epsilon = 10^{-3}$. Obtain the number of the reduced orthonormal basis p such that $\lambda_{0_1}/\lambda_{0_p} < \epsilon$.
4. Create the reduced matrix of eigenvalues and eigenvectors
$$\boldsymbol{\Lambda}_{0_p} = \mathrm{diag}\big[\lambda_{0_1}, \lambda_{0_2}, \ldots, \lambda_{0_p}\big] \in \mathbb{R}^{p\times p} \quad \text{and} \quad \boldsymbol{\Phi}_p = \big[\boldsymbol{\phi}_1, \boldsymbol{\phi}_2, \ldots, \boldsymbol{\phi}_p\big] \in \mathbb{R}^{n\times p}. \tag{69}$$
5. Calculate the transformed matrices and vector
$$\widetilde{\mathbf{A}}_i = \boldsymbol{\Phi}_p^T \mathbf{A}_i \boldsymbol{\Phi}_p \in \mathbb{R}^{p\times p}; i = 1,2,\ldots,M \quad \text{and} \quad \widetilde{\mathbf{f}} = \boldsymbol{\Phi}_p^T \mathbf{f} \tag{70}$$
and separate the diagonal and off diagonal terms as $\widetilde{\mathbf{A}}_i = \boldsymbol{\Lambda}_i + \boldsymbol{\Delta}_i$.
6. Select a number of samples, say N_{samp}. Generate the samples of (in general non-Gaussian) random variables $\xi_i(\omega)$, $i = 1,2,\ldots,M$.
7. Obtain the inverse of the diagonal matrix $\boldsymbol{\Lambda}(\xi(\omega))$ defined in Eq. (24) as
$$\boldsymbol{\Lambda}_I(\omega) = \left[\boldsymbol{\Lambda}_0^{-1} + \sum_{i=1}^{M} \xi_i(\omega)\boldsymbol{\Lambda}_i^{-1}\right] \tag{71}$$
and the trace less matrix
$$\boldsymbol{\Delta}(\omega) = \sum_{i=1}^{M} \xi_i(\omega)\boldsymbol{\Delta}_i. \tag{72}$$
8. Calculate the first-order spectral function in a vector form as
$$\widehat{\boldsymbol{\Gamma}}^{(1)}(\omega) = \boldsymbol{\Lambda}_I(\boldsymbol{\xi}(\omega))\widetilde{\mathbf{f}} \in \mathbb{R}^p. \tag{73}$$
If higher order spectral functions are necessary, then calculate the matrix
$$\mathbf{R}(\xi(\omega)) = \boldsymbol{\Lambda}_I(\xi(\omega))\boldsymbol{\Delta}(\xi(\omega)) \in \mathbb{R}^{p\times p}. \tag{74}$$
From this calculate the sth order spectral function as
$$\boldsymbol{\Gamma}^{(s)}(\xi(\omega)) = \Big[\mathbf{I}_p - \mathbf{R}(\xi(\omega)) + \mathbf{R}(\xi(\omega))^2 - \mathbf{R}(\xi(\omega))^3 + \ldots s^{\text{th term}}\Big]\boldsymbol{\Gamma}^{(1)}(\xi(\omega)) \in \mathbb{R}^p. \tag{75}$$
9. Calculate the mean vector from the generated samples
$$\overline{\boldsymbol{\Gamma}} = \mathrm{E}[\boldsymbol{\Gamma}(\omega)] \in \mathbb{R}^p. \tag{76}$$
10. Calculate the following $(1 + M)$ matrices from the samples of $\boldsymbol{\Gamma}(\omega)$
$$\mathbf{D}_0 = \mathrm{E}[\boldsymbol{\Gamma}(\omega)\boldsymbol{\Gamma}^T(\omega)] \in \mathbb{R}^{p\times p}, \tag{77}$$
$$\text{and} \quad \mathbf{D}_i = \mathrm{E}[\boldsymbol{\Gamma}(\omega)\xi_i(\omega)\boldsymbol{\Gamma}^T(\omega)] \in \mathbb{R}^{p\times p}, \quad \forall\, i = 1,2,\ldots,M. \tag{78}$$
11. Following Eq. (51), form the coefficient matrix $\mathbf{S}$ and the vector $\mathbf{b}$ as
$$\mathbf{S} = \boldsymbol{\Lambda}_{0_p} \odot \mathbf{D}_0 + \sum_{i=1}^{M} \widetilde{\mathbf{A}}_i \odot \mathbf{D}_i \in \mathbb{R}^{n\times n} \quad \text{and} \quad \mathbf{b} = \widetilde{\mathbf{f}} \odot \overline{\boldsymbol{\Gamma}} \in \mathbb{R}^n, \tag{79}$$
where $\odot$ implies element to element multiplication (as in MATLAB™ dot notation).
12. Obtain the coefficient vector
$$\mathbf{c} = \mathbf{S}^{-1}\mathbf{b} \in \mathbb{R}^p. \tag{80}$$
13. Calculate the mean of the solution
$$\bar{\mathbf{u}} = \sum_{k=1}^{p} c_k \overline{\Gamma}_k \boldsymbol{\phi}_k. \tag{81}$$
14. Obtain the covariance matrix of the spectral functions as
$$\boldsymbol{\Sigma}_\Gamma = \mathbf{D}_0 - \overline{\boldsymbol{\Gamma}}\,\overline{\boldsymbol{\Gamma}}^T. \tag{82}$$
From this calculate the covariance of the solution using Eq. (66).

In Appendix A we give a simple code in MATLAB™ to implement this computational method.

Remark 4. The computational complexity: The main computational cost of the proposed method depends on (a) the solution of the matrix eigenvalue problem (68) with reduced number of eigenvalues, (b) the generation of the $\mathbf{D}_i$ matrices in Eqs. (77) and (78), and (c) the calculation of the coefficient vector in Eq. (80). Both the matrix inversion and the matrix eigenvalue problem [39] scales in $O(p^3)$ in the worse case. The calculation of the $\mathbf{D}_i$ matrices in Eqs. (77) and (78) scales linearly with M and $p(p+1)/2$ with p. Therefore, this cost scales with $O((M+1)\,p(p+1)/2)$. The overall cost is $2O(p^3) + O((M+1)p(p+1)/2)$. For large M and p, asymptotically the computational cost becomes $C_s = O(Mp^2) + O(p^3)$. The important point to note here is that the proposed approach scales linearly with the number of random variables M. For comparison, in the classical PC expansion one needs to solve a matrix equation of dimension Pn, which in the worse case scales with $(O(Pn)^3)$. Since $P \gg M$ and $n > p$, we have $(O(P^3n^3) \gg O(Mp^2) + O(p^3)$.

7. Illustrative application: The stochastic mechanics of ZnO nanowires

In this section we apply the computational method to the nanomechanics of zinc oxide (ZnO) nanowires (NW). ZnO [40]

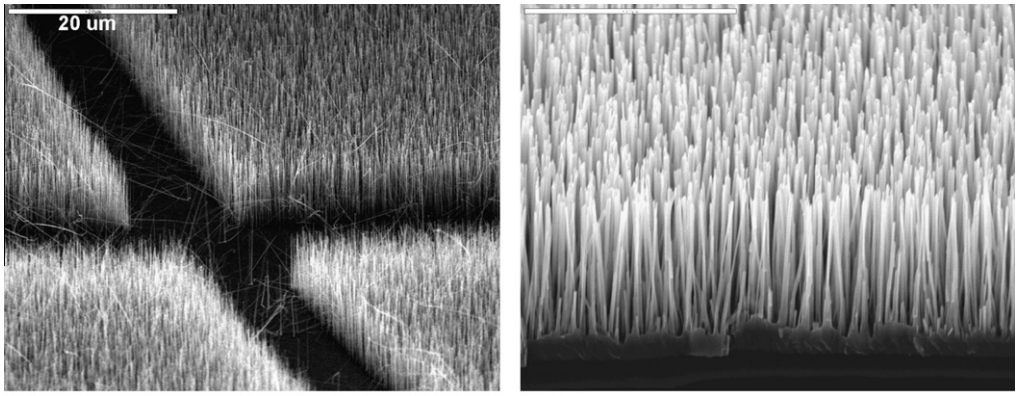

(a) A collection of vertically grown ZnO NWs. This can be viewed as the sample space for the application of stochastic finite element method.

(b) Uncertainties in ZnO NWs in the close up view. The uncertain parameter include geometric parameters such as the length and the cross sectional area along the length, boundary condition and material properties.

Fig. 1. Scanning electron microscope (SEM) image of zinc oxide (ZnO) nanowires (NW) grown on gallium nitride (GaN) substrate using the vapour transfer method. The source materials consist of commercially available ZnO and graphite powders mixed and placed at the centre of the furnace. The furnace is heated to about 975 °C, causing the ZnO powder to evaporate. The vapour is carried downstream by a flow of Ar mixed with 2% O_2 to the growth substrates where the lower temperature (600–650 °C) causes the vapour to condense into the nanowires. Significant variabilities in the NWs can be clearly observed even when they are grown in identical conditions.

materials have attracted extensive attention due to their excellent performance in electronic, ferroelectric and piezoelectric applications [41–44]. Nano-scale ZnO is also an important material [45,46] for the nanoscale energy harvesting and scavenging [47–50]. Investigation and understanding of the bending of ZnO nanowires are valuable for their potential application. For example, ZnO nanowires are bend by rubbing against each other for energy scavenging [47–50]. These studies show that for the future nano energy scavenging devices several thousands of ZnO NWs will be used simultaneously. This gives a natural framework for the application of stochastic finite element method due to a large 'sample space'. ZnO NWs have the nano piezoelastic property so that the electric charge generated is a function of the deformation [47–51]. It is therefore vitally important to look into the ensemble behavior of the deformation of ZnO NW for the reliable estimate of mechanical deformation and consequently the charge generation. For the nano-scale application this is especially crucial as the margin of error is very small. Here we study the deformation of a cantilevered ZnO NW with stochastic properties under the atomic force microscope (AFM) tip.

SEM images of ZnO NWs grown on Gallium Nitride (GaN) substrate (in Swansea University's Multidisciplinary Nanotechnology Centre) is shown in Fig. 1. One can observe significant variability within ZnO NWs even when they are grown on the same substrate and under identical conditions. This inevitable variability, the large sample space and the need for precise predictions are the key motivations for applying the stochastic finite element to this problem. We consider large NWs of lengths in excess of hundreds of nanometers. Molecular dynamic simulations of such large systems are extremely expensive. We use Euler–Bernoulli beam model validated by Gao and Wang [52]. Nanowires, unlike nanotubes, have solid cross sections. In Fig. 2, form the SEM image as well as from the atomistic model one can observe that the ZnO NW has a hexagonal cross sectional area. We study the deflection of ZnO NW under the AFM tip considering stochastically varying bending modulus. The variability of the deflection is particularly important as the harvested energy from the bending depends on it.

We assume that the bending modulus of the ZnO NW is a random field of the form

$$EI(x,\omega) = EI_0(1 + a(x,\omega)), \tag{83}$$

where x is the coordinate along the length of ZnO NW, EI_0 is the estimate of the mean bending modulus, $a(x,\omega)$ is a zero mean stationary random field. Two types or random field models have been considered, namely Gaussian and uniform. The Gaussian model is considered only to compare the numerical results with the classical polynomial chaos results. The autocorrelation function of the random field is assumed to be

$$C_a(x_1,x_2) = \sigma_a^2 e^{-(|x_1-x_2|)/\mu_a}, \tag{84}$$

where μ_a is the correlation length and σ_a is the standard deviation. The random field $a(x,\omega)$ is expressed using the Karhunen–Loève expansion (3) with the eigenvalues and eigenfunctions given by Ghanem and Spanos [5]. For the first case the random variables $\xi_i(\omega)$ are considered to be independent Gaussian random variables with zero mean and unit standard deviation. In the second model the random variables $\xi_i(\omega)$ are considered to be independent uniform random variables with zero mean and unit standard deviation.

We consider a long nanowire where the continuum model has been validated [52]. We use the baseline parameters for the ZnO NW from Gao and Wang [52] as the length $L = 600$ nm, diameter $d = 50$ nm and the lateral point force at the tip $f_T = 80$ nN. Using these data, the baseline deflection can be obtained as $\delta_0 = 145$ nm. We normalize our results with this baseline value for convenience. Two correlation lengths are considered in the numerical studies, namely $\mu_a = L/2$ and $\mu_a = L/10$. For the finite element discretization, the nanowire is divided into a number of beam elements of equal length. Standard four degrees of freedom Euler–Bernoulli beam model is used [13]. To investigate the numerical aspects of the proposed methodology, the following four cases are considered:

- *Case 1:* The random field $a(x,\omega)$ is assumed to be a Gaussian random field with correlation length $\mu_a = L/2$. Four terms in the KL expansion are considered and the nanowire is divided into 300 elements. For this case we have $n = 600$ and $M = 4$. The results are compared with the classical polynomial chaos expansion.
- *Case 2:* The random field $a(x,\omega)$ is assumed to be an Uniform random field with correlation length $\mu_a = L/2$. The nanowire is divided into 300 elements and 29 uniform random variables are considered in the discretization of the random field. The

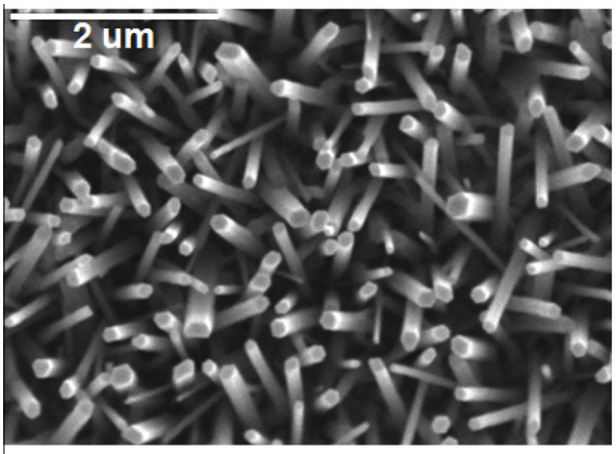

(a) The SEM image of a collection of ZnO NW showing hexagonal cross sectional area.

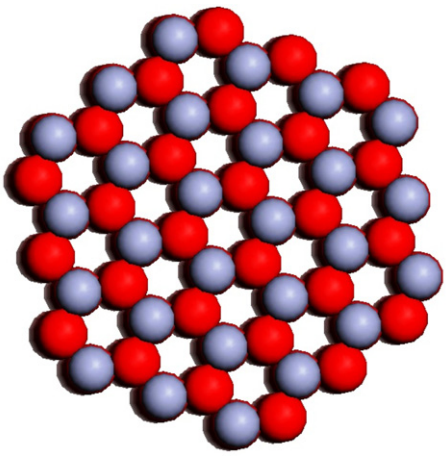

(b) The atomic structure of the cross section of a ZnO NW (the red is O_2 and the grey is Zn atom)

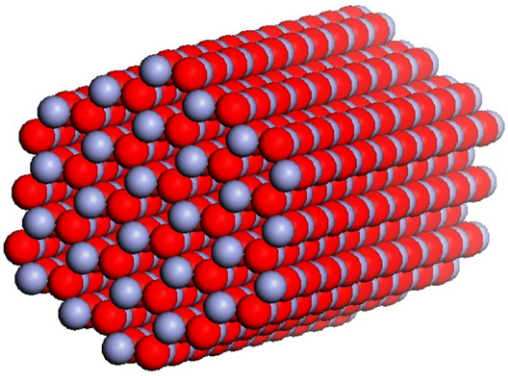

(c) The atomistic model of a ZnO NW grown from a ZnO crystal in the $(0, 0, 0, 1)$ direction.

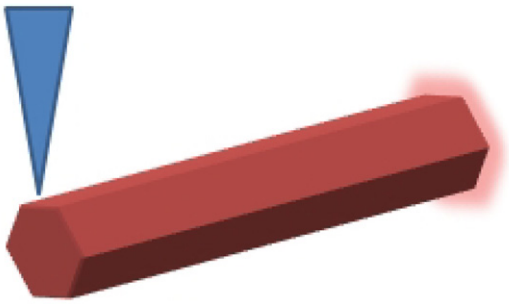

(d) The continuum idealization of a cantilevered ZnO NW under an AFM tip.

Fig. 2. The atomistic structure and equivalent continuum model of ZnO NWs. From the SEM image in (a) it can be seen that the ZnO NW has a hexagonal cross section. Unlike nanotubes, nanowires have solid cross sections (see (b) and (c)). Our aim is to study the deflection of ZnO NW under the AFM tip considering stochastically varying bending modulus. The estimate of the tip deflection is important due to the nano piezoelastic property of ZnO NWs. The electric charge generated is a function of the deformation. The baseline parameters for the ZnO NW are taken to be [52]: length $L = 600$ nm, diameter $d = 50$ nm and the lateral point force at the AFM tip $f_T = 80$ nN. The tip deflection of the baseline ZnO NW, $\delta_0 = 145$ nM.

value of M is selected such that $v_M/v_1 = 0.03$. For this case we have $n = 600$ and $M = 29$. The results are compared with the classical Neumann expansion.

- *Case 3:* The random field $a(x,\omega)$ is assumed to be an uniform random field with correlation length $\mu_a = L/2$. The nanowire is divided into 1200 elements and 29 uniform random variables are considered in the discretization of the random field as above. For this case we have $n = 2400$ and $M = 29$.
- *Case 4:* The random field $a(x,\omega)$ is assumed to be an uniform random field with a smaller correlation length $\mu_a = L/10$. The nanowire is divided into 1200 elements and 111 uniform random variables are considered in the discretization of the random field. For this case we have $n = 2400$ and $M = 111$.

7.1. Case 1: Comparison with classical polynomial chaos results

The quantity $E(x,\omega)$ in Eq. (83) should be positive for all x and $\omega \in \Omega$. Therefore, the Gaussian random field is not an ideal model for $E(x,\omega)$. However, due to the small values of σ_a (maximum of $\sigma_a = 0.2$ is considered), the probability that $E(x,\omega)$ is negative is small. We have verified that all the realizations of $E(x,\omega)$ are physical in nature in our Monte Carlo simulation. This case is considered only to compare the results with classical polynomial chaos expansion. The approach proposed in the paper is applicable to general non-Gaussian random field as considered in the next subsections.

To apply the proposed method, we need to obtain the reduced orthonormal basis by solving the eigenvalue problem involving the stiffness matrix $\mathbf{A}_0$. In Fig. 3, the eigenvalues and eigenvectors of the stiffness matrix $\mathbf{A}_0$ are shown. For $\epsilon = 0.01$, the number of reduced eigenvectors p is calculated such that $\lambda_{0_1}/\lambda_{0_p} < \epsilon$. For this problem we obtain $p = 6$. The first 300 eigenvalues and the selected six eigenvalues are shown in Fig. 3(a). The ratio of the first eigenvalue to the other eigenvalues, that is, $\lambda_{0_1}/\lambda_{0_j}$, for the first 300 eigenvalues are shown in. The eigenvectors corresponding to the first six eigenvalues are plotted in Fig. 3(b). Only the transverse degrees of freedom (DOF) is shown as we are interested in the tip deflection of the nanowire. For the polynomial chaos (PC) expansion, 4th order PC has been used. For $M = 4$ and $r = 4$, from Eq. (12) we have the number of terms in the PC expansion $P = 70$. Since $n = 600$, the total number of unknowns to be solved for the PC approach is $Pn = 42{,}000$. For the proposed Galerkin method with six eigenvectors, one only seed to solve only a 6×6 Eq. (80) to obtain the unknown coefficients.

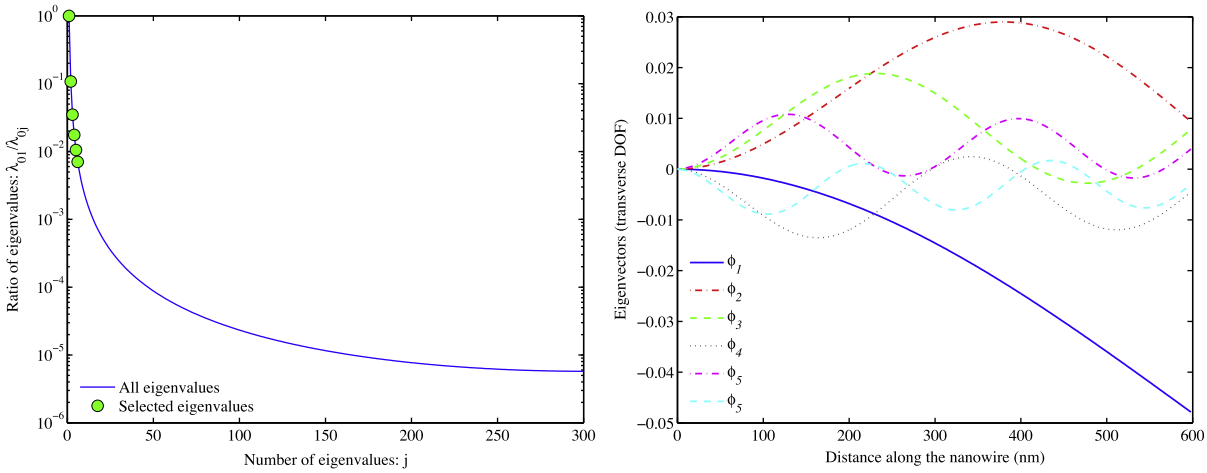

(a) Ratio of eigenvalues of the stiffness matrix $\mathbf{A}_0$. (b) First six eigenvectors of $\mathbf{A}_0$ (transverse DOF).

Fig. 3. The eigenvalues and eigenvectors of the stiffness matrix $\mathbf{A}_0$. For $\epsilon = 0.01$, the number of reduced eigenvectors $p = 6$ such that $\lambda_{0_1}/\lambda_{0_p} < \epsilon$.

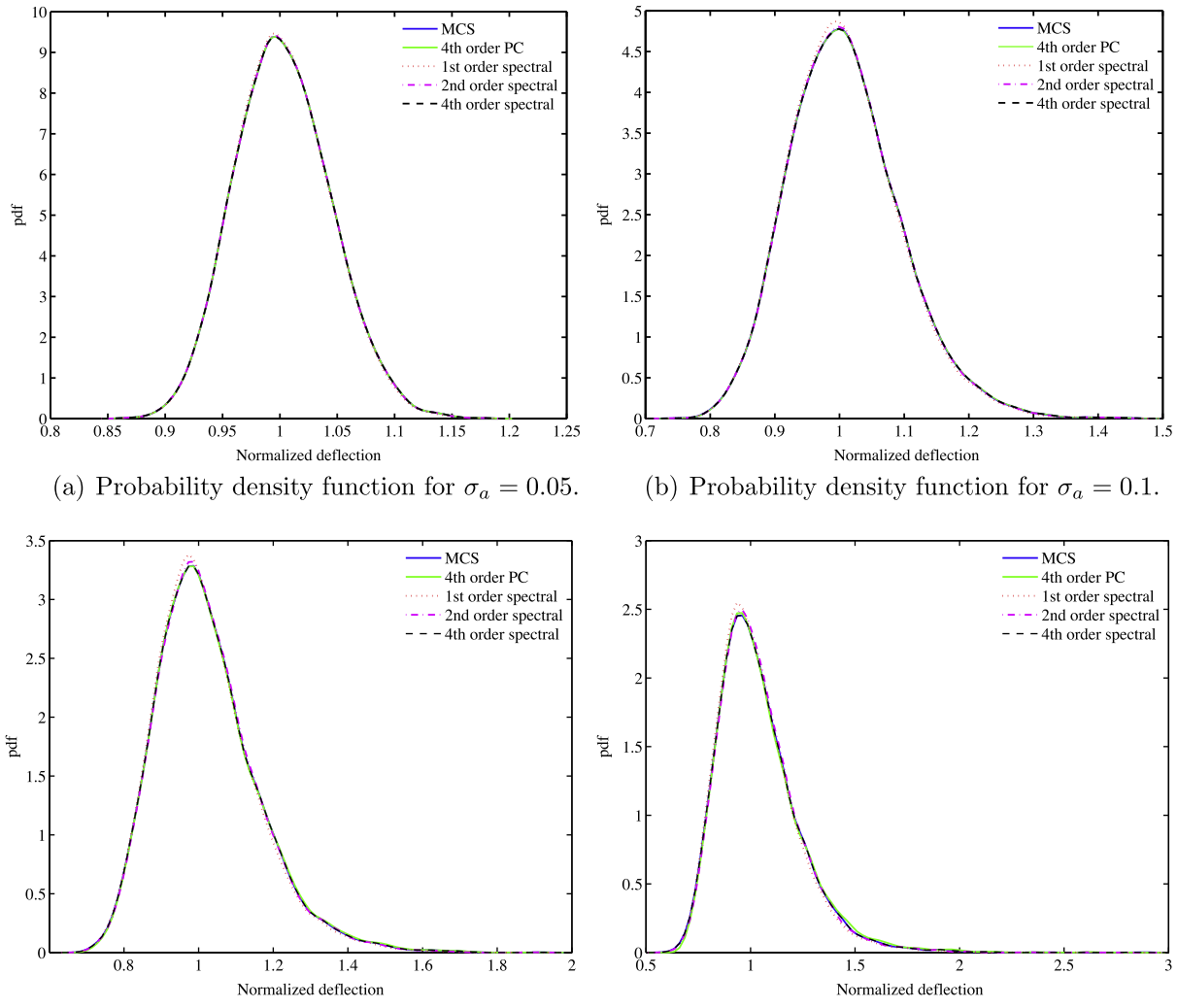

(a) Probability density function for $\sigma_a = 0.05$. (b) Probability density function for $\sigma_a = 0.1$.

(c) Probability density function for $\sigma_a = 0.15$. (d) Probability density function for $\sigma_a = 0.2$.

Fig. 4. The probability density function of the normalized deflection δ/δ_0 of the ZnO NW under the AFM tip ($\delta_0 = 145$ nm). The pdfs are obtained with 10,000 sample MCS and for $\sigma_a = \{0.05, 0.10, 0.15, 0.20\}$. For $n = 600$ and $M = 4$, the fourth-order PC needs solution of a linear system of equation of size 42,000. In comparison the proposed Galerkin approach needs solution of a linear system of equation of size six only. The average computational time for the five methods shown are – direct MCS: 43.2131 min; PC: 16.8559 min; first order spectral: 2.8860 s; 2nd order spectral: 3.2448 s; and fourth order spectral: 3.2604 s.

The method outlined in Section 6.2 is applied with 10,000-sample Monte Carlo simulation (MCS). The MATLAB™ function developed for this purpose is listed in Appendix. The computer programs were run in a twin Intel Xeon X5355 (2.67 GHz) processor machine with 16 GB RAM. The probability density function of the normalized deflection is shown Fig. 4 for the four values of σ_a. We consider $\sigma_a = \{0.05, 0.10, 0.15, 0.20\}$ to simulate increasing uncertainty. First, second and fourth-order spectral functions have been used. It can be observed that the results from the proposed reduced orthonormal basis approach match the direct MCS and PC results very well. The full MCS and PC takes 43.2131 min and 16.8559 min, respectively, while the first, second and fourth order spectral methods take only 2.8860, 3.2448 and 3.2604 s, respectively. This also shows that higher-order spectral functions can be used with very little additional computational cost. This is due to the fact that, unlike the PC approach, the number of equations to be solved in the Galerkin step does not increase with the increase in the order of the spectral functions. The actual computational times given here are for illustrative purpose only. These values will change significantly based on the computing hardware and basic numerical algorithms (e.g., eigenvalue solver, solution of system of linear equations etc.). Here MATLAB™ has been used to perform all calculations. Although the actual computational times will change, the relative timings may not change significantly provided they are implemented in a consistent manner. Therefore, the computational times reported in this paper should be viewed as guidelines as opposed to true time one may need in order to repeat this study elsewhere.

Table 1
Percentage errors in the mean and standard deviation of the tip deflection of the ZnO NW with Gaussian random field model. The direct MCS results are used as the reference solution. The fourth-order spectral method turns out to be the most accurate, followed by the fourth-order PC.

Statistics	Methods	$\sigma_a = 0.05$	$\sigma_a = 0.10$	$\sigma_a = 0.15$	$\sigma_a = 0.20$
Mean	Fourth order PC	0.0864	0.0267	0.1041	0.1462
	First order spectral	0.0603	0.2289	0.5384	1.0589
	Second order spectral	0.0048	0.0062	0.0140	0.0454
	Fourth order spectral	0.0047	0.0048	0.0053	0.0069
Standard deviation	Fourth order PC	0.7143	0.9065	1.4948	0.1800
	First order spectral	1.1871	1.6784	3.0980	5.1614
	Second order spectral	0.1011	0.5166	1.4668	3.2479
	Fourth order spectral	0.0179	0.0153	0.0004	0.0886

In Table 1 we show percentage errors in the mean and standard deviation of the tip deflection. The first-order spectral method is the least accurate and the fourth-order spectral method the most accurate method. In general the fourth-order spectral method turns out to be more accurate compared to the fourth-order PC. The fourth-order spectral method requires 3.2604 seconds while the fourth-order PC requires 16.8559 min, which implies that the proposed method is about 310 times faster for this problem. As mentioned before, the main reason for this significant reduction in computation time is that only a 6×6 linear system is required to be solved for the proposed approach while a $42{,}000 \times 42{,}000$ system is required to be solved for the PC approach. Although we are directly comparing the proposed spectral approach with the classical PC, it should be remembered that very different basis are used in the two approaches. In addition it should be noted that the classical PC approach does not use the spectral reduction based on the p-dimensional dominant eigenspace of the operator $\mathbf{A}_0$. The computational times given here should be viewed in the light of these points.

For $p = 6$ the proposed fourth-order spectral approach is already more accurate than the fourth-order polynomial chaos approach. Our numerical studies show that the further increase in the value of p does not change the results significantly. Therefore, we use $p = 6$ in the next sections where a non-Gaussian random field model with more number of random variables are considered.

7.2. Case 2: Comparison with classical Neumann expansion

The hybrid analytical-simulation method proposed here is compared with the classical Neumann expansion. In Fig. 7 the mean and standard deviation of the normalized deflection δ/δ_0 of the ZnO NW under the AFM tip are shown. In Fig. 5 the mean and standard deviation of the normalized deflection δ/δ_0 of the ZnO NW under the AFM tip are shown. Here 29 uncorrelated uniform

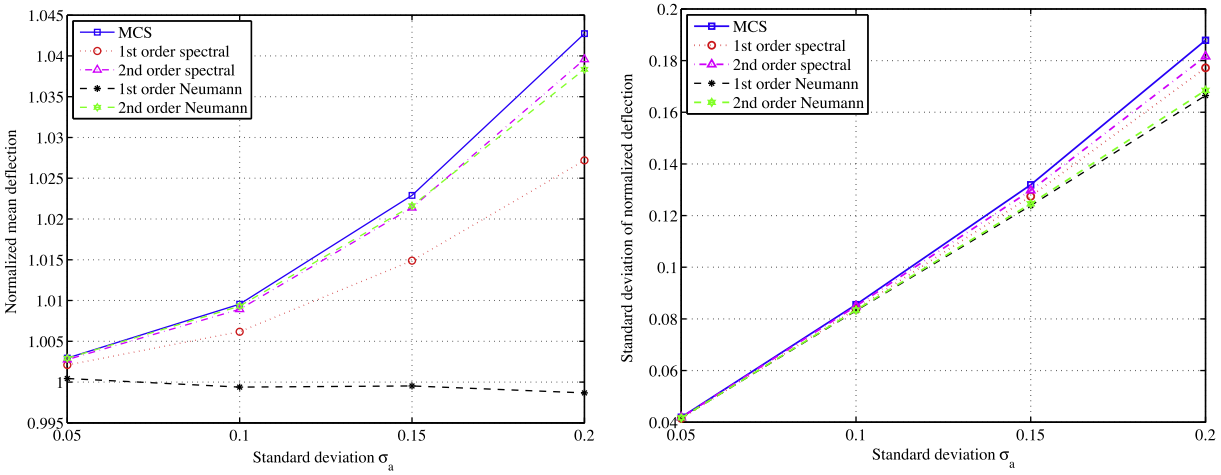

(a) Mean of the normalized deflection. (b) Standard deviation of the normalized deflection.

Fig. 5. The mean and standard deviation of the normalized deflection δ/δ_0 of the ZnO NW under the AFM tip with uniform random field. The correlation length of the random field describing the bending rigidity is assumed to be $\mu_a = L/2$. The classical Neumann expansion method is compared with the proposed reduced spectral method with Galerkin projection.

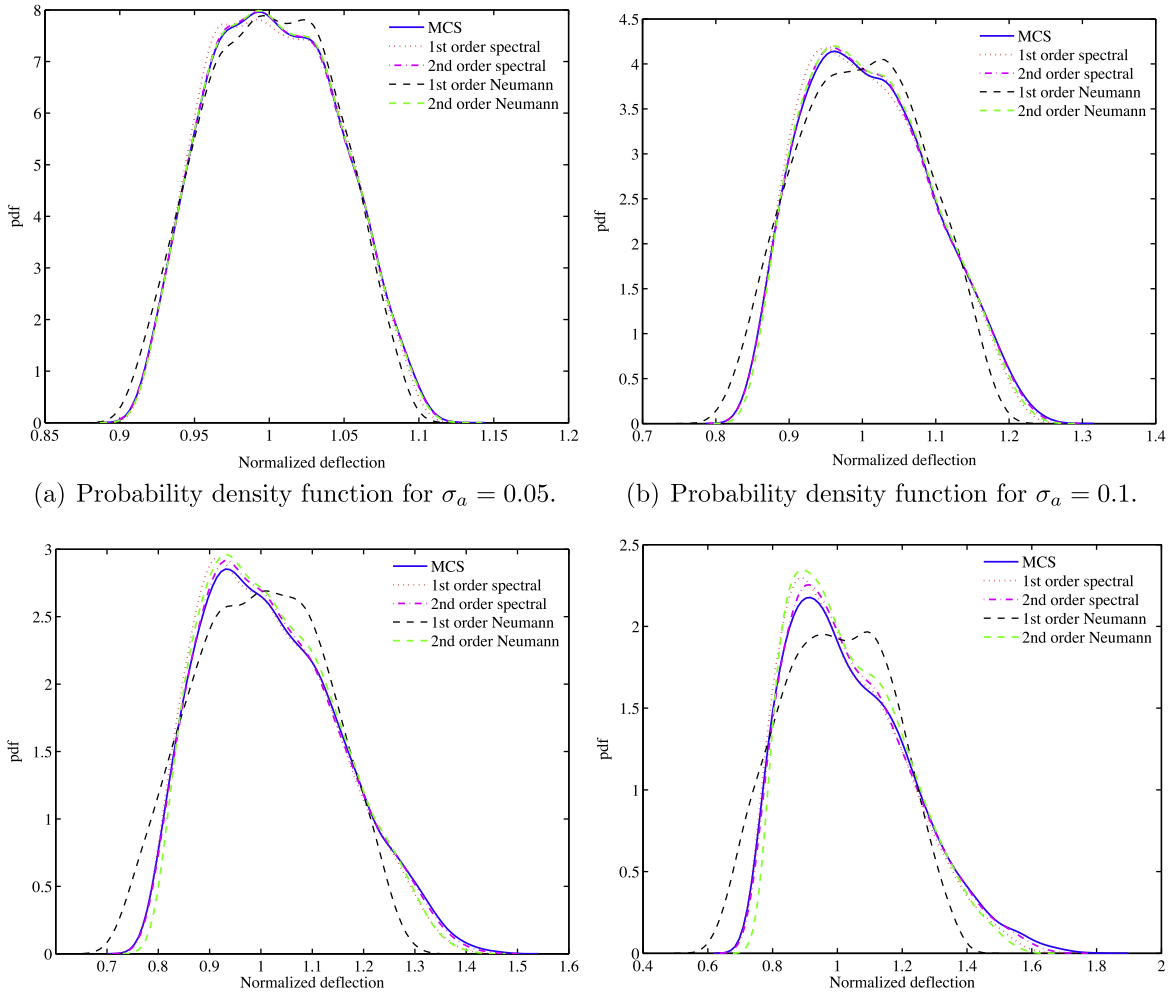

(a) Probability density function for $\sigma_a = 0.05$. (b) Probability density function for $\sigma_a = 0.1$.

(c) Probability density function for $\sigma_a = 0.15$. (d) Probability density function for $\sigma_a = 0.2$.

Fig. 6. The probability density function of the normalized deflection δ/δ_0 of the ZnO NW under the AFM tip (δ_0 = 145 nm). The pdfs are obtained with 10,000 sample MCS and for $\sigma_a = \{0.05, 0.10, 0.15, 0.20\}$, $n = 300$ and $M = 29$. The classical Neumann expansion method is compared with the proposed reduced spectral method with Galerkin projection.

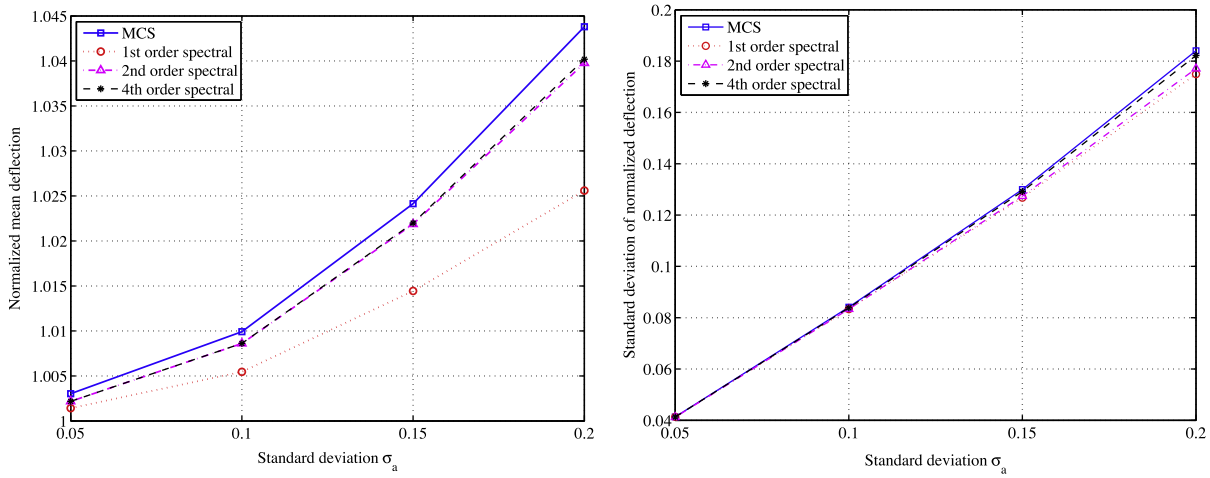

(a) Mean of the normalized deflection. (b) Standard deviation of the normalized deflection.

Fig. 7. The mean and standard deviation of the normalized deflection δ/δ_0 of the ZnO NW under the AFM tip with uniform random field. The correlation length of the random field describing the bending rigidity is assumed to be $\mu_a = L/2$.

random variables have been used to generate the bending rigidity random field. We again consider $\sigma_a = \{0.05, 0.10, 0.15, 0.20\}$ to simulate increasing uncertainty. This is done to check the accuracy of the proposed method against the classical Neumann expansion. The probability density function of the normalized deflection is shown Fig. 6 for the four values of σ_a. First and second-order spectral function approaches are compared with the first and second order Neumann expansion. It can be observed that the results from the proposed reduced orthonormal basis approach are more accurate compared to the corresponding order Neumann expansion method. The difference is more prominent when the standard deviation of the input random field is higher. This is due to the fact that, unlike the Neumann expansion, the proposed method uses Galerkin approach for error minimization.

Table 2
Percentage errors in the mean and standard deviation of the tip deflection of the ZnO NW with uniform random field and correlation length $\mu_a = L/2$ ($n = 2400$ and $M = 29$). The direct MCS results are used as the reference solution. The first, second and fourth order spectral function with proposed Galerkin approach are considered and the direct MCS is used as the reference solution.

Statistics	Methods	$\sigma_a = 0.05$	$\sigma_a = 0.10$	$\sigma_a = 0.15$	$\sigma_a = 0.20$
Mean	First order spectral	0.1602	0.4415	0.9475	1.7444
	Second order spectral	0.0845	0.1303	0.2211	0.3867
	Fourth order spectral	0.0845	0.1285	0.2105	0.3458
Standard deviation	First order spectral	0.0350	0.9037	2.4522	4.9665
	Second order spectral	0.2958	0.8689	1.9842	3.7927
	Fourth order spectral	0.1642	0.3030	0.5618	1.0063

7.3. Case 3: Uniform random field with larger correlation length

The hybrid analytical-simulation method proposed here is compared with the direct MCS obtained by solving Eq. (6) for each sample. In Fig. 7 the mean and standard deviation of the normalized deflection δ/δ_0 of the ZnO NW under the AFM tip are shown. Here 29 uncorrelated uniform random variables have been used to generate the bending rigidity random field. We again consider $\sigma_a = \{0.05, 0.10, 0.15, 0.20\}$ to simulate increasing uncertainty. This

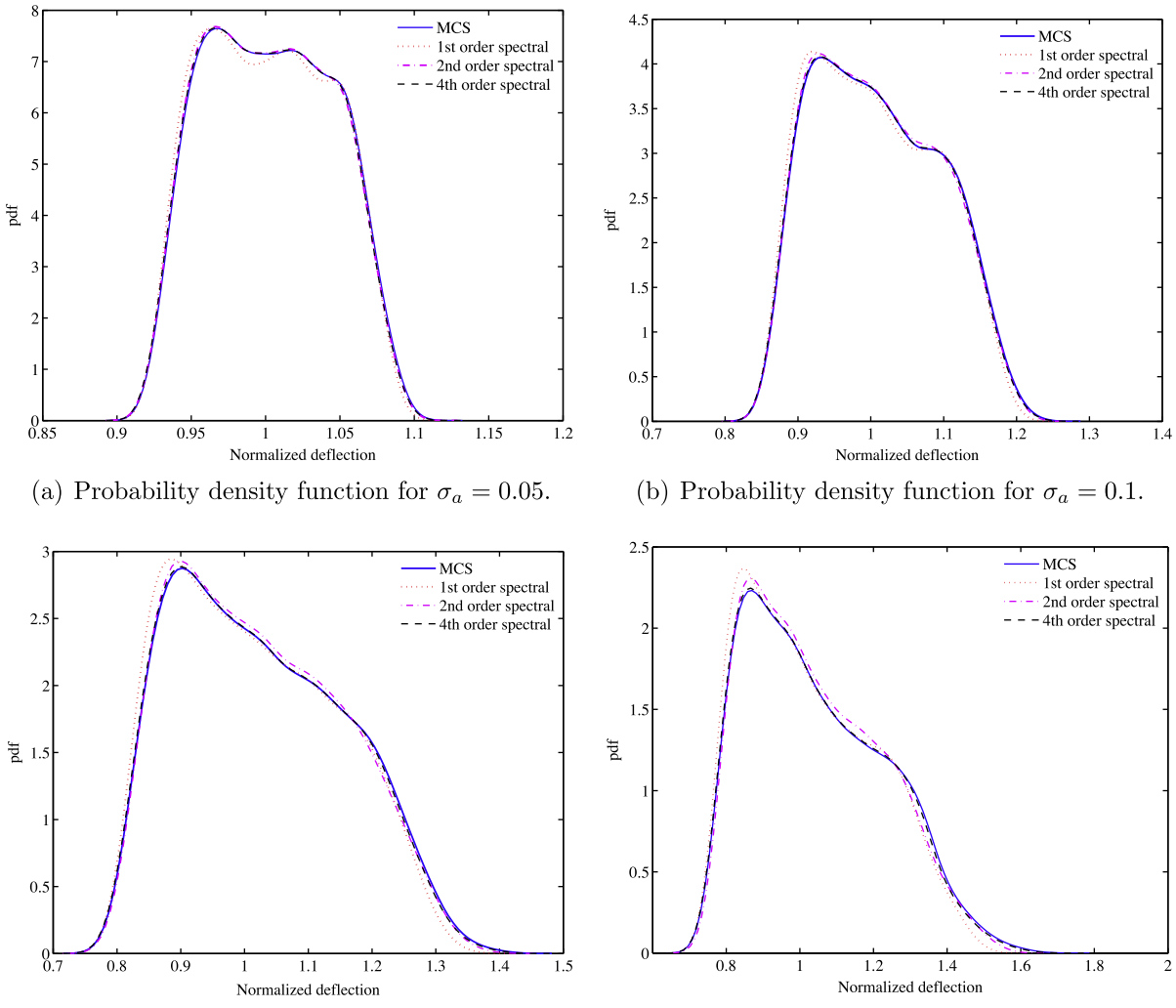

(a) Probability density function for $\sigma_a = 0.05$.

(b) Probability density function for $\sigma_a = 0.1$.

(c) Probability density function for $\sigma_a = 0.15$.

(d) Probability density function for $\sigma_a = 0.2$.

Fig. 8. The probability density function of the normalized tip deflection of the ZnO NW with uniform random field. The pdfs are obtained with 10,000 sample MCS and four values of σ_a have been used. For $n = 2400$ and $M = 29$ the first, second and fourth-order PC method would need the solution of a linear system of equation of dimension 72,000, 1.116 million and 98.208 million respectively. In comparison the proposed Galerkin approach needs solution of a linear system of equation of dimension six only. The average computational time for the four methods shown are – direct MCS: 19.2590 h; first order spectral: 109.6687 s; second order spectral: 112.7731 s; and fourth order spectral: 116.6419 s. The fourth-order spectral approach is the closest to the direct MCS results.

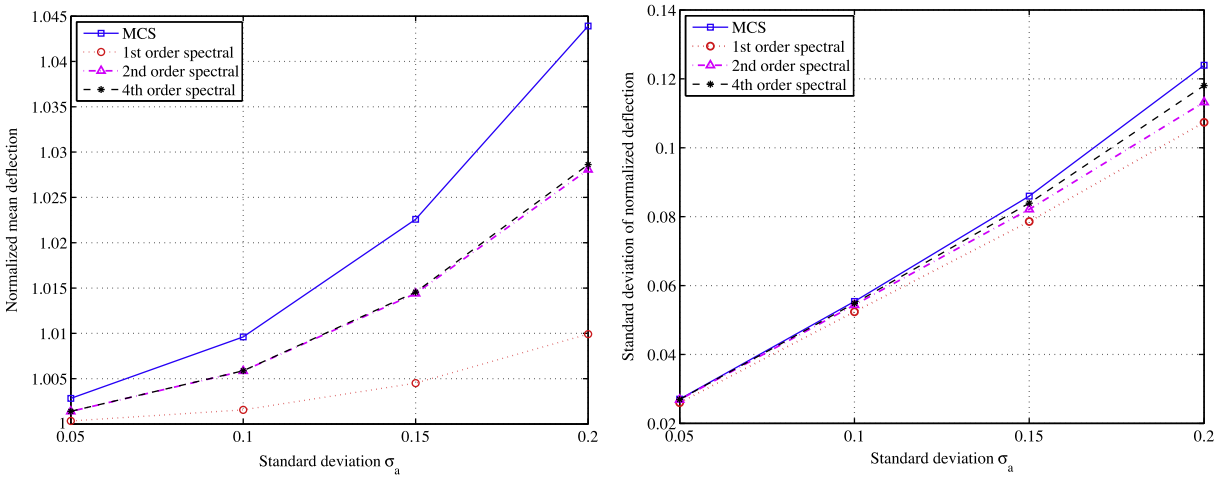

(a) Mean of the normalized deflection. (b) Standard deviation of the normalized deflection.

Fig. 9. The mean and standard deviation of the normalized tip deflection of the ZnO NW with uniform random field. The correlation length of the random field describing the bending rigidity is assumed to be $\mu_a = L/10$.

is done to check the accuracy of the proposed method against the direct MCS results. Like the previous examples, the first six eigenvalues and eigenvectors are used for the proposed reduced spectral method. It can be seen that the results from the three spectral functions in conjunction with the Galerkin approach produce accurate results for all the four values of σ_a. Percentage errors corresponding to this figure are shown in Table 2. The probability density function of the normalized deflection is shown Fig. 8 for the four values of σ_a. As expected, the error corresponding to the fourth-order spectral function approach is smaller than the other two approaches. The difference between the computational cost for the first, second and fourth-order approach is small as in average they take 109.6687, 112.7731 and 116.6419 s, respectively. Compared to this, the direct MCS takes 19.2590 h of CPU time.

For the first-order approach, the vector containing the spectral functions is obtained from Eq. (73). For the second and fourth-order approaches, this vector is obtained from Eq. (75) with two and four terms, respectively. The rest of the procedure to obtain the response statistics is identical. Therefore, the only additional computational expense is matrix vector multiplications of dimension $p = 6$ for this case. In this problem the size of the system $n = 2400$ and the number of random variables $M = 29$. If the polynomial chaos method was used, then from Eq. (12) one obtains the value of P as 30, 465 and 40,920 for the first, second and fourth order PC. This implies that one would need to solve a linear system of equation of size 72,000, 1.116 million and 98.208 million, respectively. For the proposed reduced Galerkin approach only a set of six equations are solved to obtain the coefficients. This shows the computational efficiency of this approach without loosing significant accuracy.

7.4. Case 4: Uniform random field with smaller correlation length

For correlation length $\mu_a = L/10$, we have used $M = 111$ number of uncorrelated uniform random variables to generate the bending rigidity random field. The method developed in the paper is applied with 10,000-sample Monte Carlo simulation (MCS). In Fig. 9 the mean and standard deviation of the normalized deflection δ/δ_0 of the ZnO NW under the AFM tip are shown for four values of σ_a. We again use the first six eigenvalues and eigenvectors for the proposed reduced spectral method. It can be seen that the results from the fourth-order spectral functions in conjunction with the Galerkin approach produce accurate results for all the four values of σ_a even when the number of random variables are large. The computation cost for the first, second and fourth-order approach is small as in average they take 137.6085, 140.9937 and 142.7097 s respectively. For this problem the direct MCS takes 37.1910 h of CPU time. Compared to the previous case with 29 random variables, the computational time for the proposed approach increase only slightly even when 111 number of random variables are used. Percentage error corresponding to the moments shown in Fig. 9 are given in Table 3. The probability density function of the normalized deflection is shown Fig. 10 for the four values of σ_a. As expected, the error corresponding to the fourth-order spectral function approach is smaller than the other two approaches. For this problem the size of the system $n = 2400$ and the number of random variables $M = 111$. If the polynomial chaos method was used, then from Eq. (12) one obtains the value of P as 112, 240, 464 and 6.91334 million for the first, second and fourth order PC. This implies that one would need to solve a linear system of equation of size 268,800, 577.1136 million and 16.5920 billion respectively. For the proposed reduced Galerkin approach only a set of six equations are solved to obtain the coefficients. Overall, when such a large number of random variables are used, the accuracy is slightly less compared to the previous case where relatively smaller number of random variables are used. The computational cost increase only slightly with the increase in the number of random variables. This is due to the fact that the increase in the number of random variables only increases the number of $\mathbf{D}_i$ matrices in Eq. (78). Unlike

Table 3
Percentage errors in the mean and standard deviation of the tip deflection of the ZnO NW with uniform random field and correlation length $\mu_a = L/10$ ($n = 2400$ and $M = 111$). The direct MCS results are used as the reference solution.

Statistics	Methods	$\sigma_a = 0.05$	$\sigma_a = 0.10$	$\sigma_a = 0.15$	$\sigma_a = 0.20$
Mean	First order spectral	0.2488	0.7974	1.7671	3.2555
	Second order spectral	0.1434	0.3725	0.8007	1.5174
	Fourth order spectral	0.1432	0.3697	0.7854	1.4641
Standard deviation	First order spectral	3.7039	5.4718	8.5930	13.3714
	Second order spectral	0.4704	1.8630	4.4737	8.6448
	Fourth order spectral	0.2561	0.9733	2.3849	4.7576

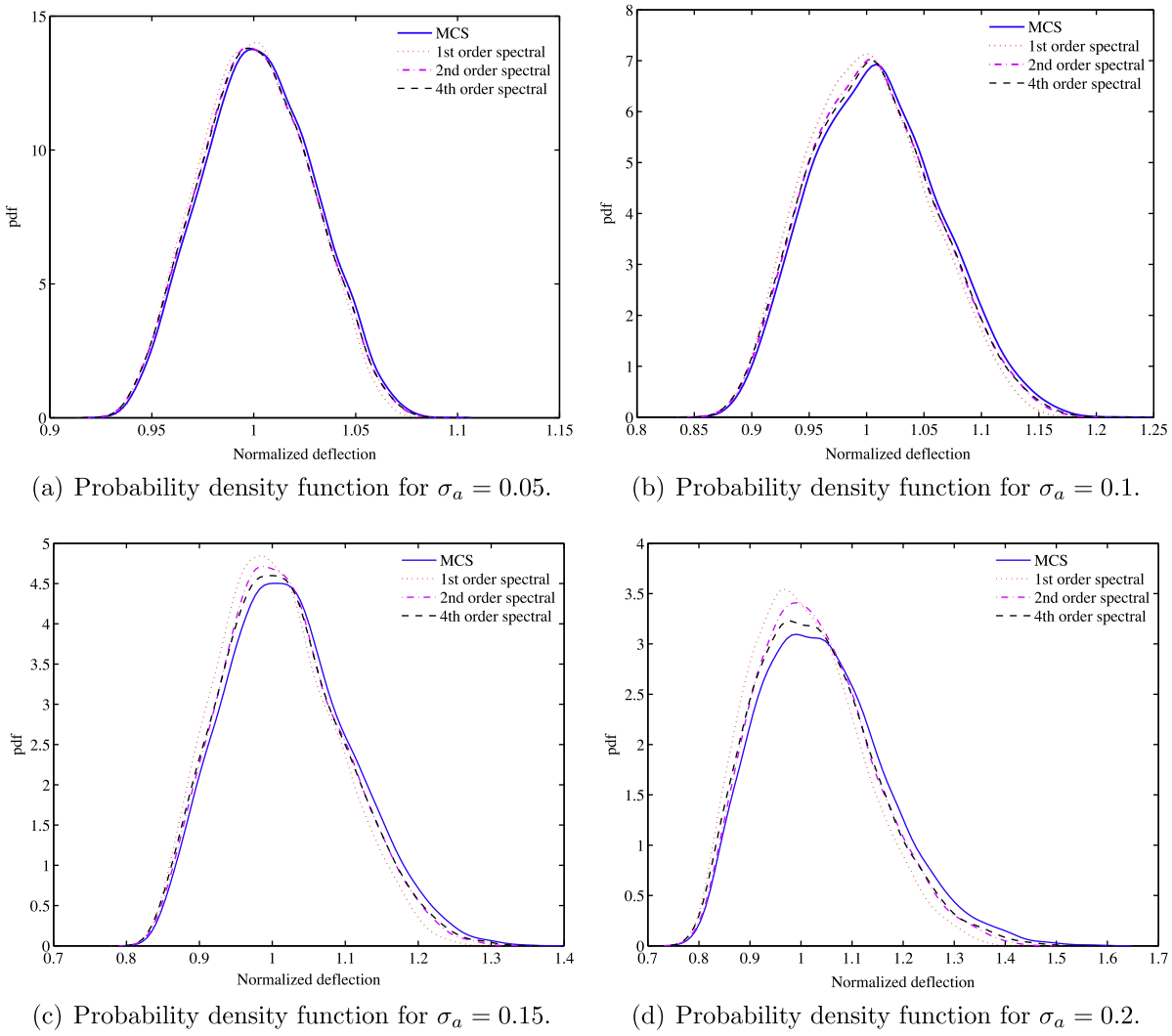

(a) Probability density function for $\sigma_a = 0.05$.

(b) Probability density function for $\sigma_a = 0.1$.

(c) Probability density function for $\sigma_a = 0.15$.

(d) Probability density function for $\sigma_a = 0.2$.

Fig. 10. The probability density function of the normalized tip deflection of the ZnO NW with uniform random field. For $n = 2400$ and $M = 111$ the first, second and fourth-order PC method would need the solution of a linear system of equation of dimension 268,800, 577.1136 million and 16.5920 billion, respectively. In comparison the proposed Galerkin approach needs solution of a linear system of equation of dimension six only. The average computational time for the four methods shown are – direct MCS: 37.1910 h; first order spectral: 137.6085 s; second order spectral: 140.9937 s; and fourth order spectral: 142.7097 s.

the polynomial chaos approach, it does not increase the number of linear equations to be solved in the Galerkin approach. The results obtained here demonstrate the computational efficiency of the proposed approach for large number of random variables without a significant loss of accuracy.

8. Conclusions

We consider discretized stochastic elliptic partial differential equations with non-Gaussian random fields. In the classical spectral stochastic finite element approach, the solution is projected into an infinite dimensional orthonormal basis functions and the associated constant vectors are obtained using the Galerkin type of error minimization approach. Here an alternative approach is proposed. The solution is projected into a finite dimensional reduced orthonormal vector basis and the associated coefficient functions are obtained. The coefficient functions, called as the *spectral functions*, are expressed in terms of the spectral properties of the matrices appearing in the discretized governing equation. It is shown that then the resulting series converges to the exact solution in probability 1. This is a stronger convergence compared to the classical polynomial chaos which converges in the mean-square sense in the Hilbert space. Using an analytical approach, it is shown that the proposed spectral decomposition has the same functional form as the exact solution, which is not a polynomial, but a ratio of polynomials where the denominator has a higher degree than the numerator.

Using the spectral functions, a Galerkin error minimization approach has been developed in a reduced orthonormal vector basis. It is shown that the number of unknown constants can be obtained by solving a system of linear equations which has a dimension much smaller than the dimension of the original discretized equation. A simple numerical approach to obtain the reduced dimension has been suggested based on the ratio of the eigenvalues of the stiffness matrix corresponding to the baseline model. A numerical approach using a general-order spectral function has been developed. Based on these, a hybrid analytical-simulation approach is proposed to obtain the statistical properties of the solution. If p is the size of the reduced system and M is the number of random variables, then the computational complexity of the proposed approach grows in $O(Mp^2) + O(p^3)$ in the worse case.

The method is applied to the stochastic nanomechanics of a ZnO nanowire under an AFM tip for illustration. First, the statistics of the tip deflection were obtained with 4 Gaussian random variables

and 600 degrees of freedom. A comparison with the classical fourth-order polynomial chaos approach shows that the proposed method using the fourth-order spectral function is more accurate and computationally efficient. A comparison with the classical Neumann expansion reveals that the proposed method is more accurate for a given order of approximation. Later the method is applied to a 2400 degrees of freedom problem with 29 and 111 number of uniform random variables. Promising accuracy compared to the direct Monte Carlo simulation, especially with the fourth-order spectral function has been observed. A fourth-order polynomial chaos approach for this problem would require the solution of linear equations of size 16.5920 billion.

```
% This function generates the samples of the solution of an elliptic SPDE
% using the projection in a reduced orthonormal vector basis
%  ---------------- Inputs----------------------
% A0 is n x n matrix
% A_i is n x n x M matrix of coefficients
% f is the n x 1 forcing vector
% Utype is the type of input random variables (1=> Gaussian, 2=> Uniform)
% nsamp is the number of samples
% RFstd is the standard deviation of the random field
% n is the dimension of the system
% M is the number of random variables
% p is the number of reduced vectors
% ApproxOrder is the order of the spectral functions
% This code is for ApproxOrder>1; comment lines 69 to 77 if only
% first-order spectral function is necessary.
%  ---------------- Outputs----------------------
% U_hat is the sample of the solutions
% GammaFn contains the samples of spectral function
% S & b are the matrix and the vector arising in the Galerkin method
%-------------------------------------------------------------------------
function[U_hat,GammaFn,S,b]=...
    spectral_orthonormal(A0,A_i,f,Utype,nsamp,RFstd,n,M,eps,ApproxOrder);

[Phi_all,Lamda0_all]=eig(A0);
Lamda0_diag=diag(Lamda0_all);

% Obtain the number of reduced orthonormal basis
ratioval=100;p=0;
while ratioval > eps
    p=p+1;
    ratioval=Lamda0_diag(1)/Lamda0_diag(p);
end

Lamda0=Lamda0_diag(1:p);
Phi=Phi_all(:,1:p);
tilde_A_i=zeros(p,p,M);Delta_i=zeros(p,p,M);lambda_i=zeros(p,M);
tilde_f=Phi'*f;
for i=1:M
    tilde_A_i(:,:,i)=Phi'*A_i(:,:,i)*Phi;
    Delta_i(:,:,i)=tilde_A_i(:,:,i);
    lambda_i(:,i)=diag(tilde_A_i(:,:,i));
    for k=1:p
        Delta_i(k,k,i)=0;
    end
end

% Any random variables can be used here: we only give Gaussian and uniform
% as examples
if Utype ==1
    % Generate iid Gaussian random variables (zero mean, unit std)
    randn('state',17); xi=randn(nsamp,M);   xi=xi*RFstd;
elseif Utype ==2
    % Generate iid Uniform random variables (zero mean, unit std)
    a=-sqrt(3);b=sqrt(3);
    rand('state',17); xi=a + (b-a).*rand(nsamp,M);   xi=xi*RFstd;
end
```

Listing 1. Code for generating samples of the solution vector.

```
57
58 % Generate the spectral functions for all samples
59 GammaFn=zeros(p,nsamp);
60 for j_samp=1:nsamp
61     td=zeros(p,1);Delta=zeros(p,p);Gamma1=zeros(p,1);
62     R=zeros(p,p);T=zeros(p,ApproxOrder);
63     for i=1:M
64         td=td+xi(j_samp,i)*lambda_i(:,i);
65         Delta=Delta+xi(j_samp,i)*Delta_i(:,:,i);
66     end
67     dLambda=Lamda0+td;
68     Gamma1=tilde_f./dLambda; % first-order spectral function
69     for j=1:p
70         for k=1:p
71             R(j,k)=Delta(j,k)/dLambda(j);
72         end
73     end
74     T(:,1)=-R*Gamma1;
75     for ia=2:ApproxOrder
76         T(:,ia)=-R*T(:,ia-1);
77     end
78     GammaFn(:,j_samp)=Gamma1+sum(T,2);
79 end
80 % Generate matrices for the Galerkin
81 GammaBar=mean(GammaFn,2);
82 D0=cov(GammaFn')+GammaBar*GammaBar';
83 D=zeros(p,p,M);
84 for j=1:p
85     for k=1:p
86         for i=1:M
87             D(j,k,i)=mean(GammaFn(j,:).'.* xi(:,i) .* GammaFn(k,:).');
88         end
89     end
90 end
91 tS=zeros(p,p);
92 for i=1:M
93     tS=tS+tilde_A_i(:,:,i) .* D(:,:,i);
94 end
95 b=GammaBar .* tilde_f;
96 S= diag(Lamda0).*D0 + tS;
97 c=S\b;
98 % Sum the series to obtain the solution
99 U_hat=zeros(n,nsamp);
100 for j_samp=1:nsamp
101     tU_hat=zeros(n,1);
102     for k=1:p
103         tU_hat=tU_hat+c(k)*GammaFn(k,j_samp)* Phi(:,k);
104     end
105     U_hat(:,j_samp)=tU_hat;
106 end
```

Listing 1 (*continued*)

The computational efficiency of the proposed reduced spectral approach has been demonstrated for large linear systems with non-Gaussian random variables. It may be possible to extend the underlying idea to non-linear and time varying problems. For example, the proposed spectral approach can be used for every linearisation step or every time step. Further research is necessary in this direction.

Acknowledgements

Dr. T.G.G. Maffeis from the Multidisciplinary Nanotechnology Centre in Swansea University is acknowledged for the SEM images of ZnO. We acknowledge R. Choudhury for the atomistic modeling of ZnO. The financial support from The Leverhulme Trust through the award of the Philip Leverhulme Prize and The Royal Society of London through the Wolfson Research Merit award is greatly acknowledged.

Appendix A. Matlab code for the implementation of the proposed numerical method

In this section we give a code in MATLAB™ (see Listing 1) to realize the computational method given in Section 6.2. The method is implemented via a MATLAB™ function which takes $\mathbf{A}_0 \in \mathbb{R}^{n\times n}, \mathbf{A}_i \in \mathbb{R}^{n\times n}, i = 1, 2, \ldots, M, \mathbf{f} \in \mathbb{R}^n$ and the number of samples as the input and returns the samples of the solution vector as the output. Only Gaussian and uniform input random variables are used (line 47–56). This can be changed to any other random variables. In the

polynomial chaos approach, one has to change the orthogonal polynomial basis based on the random variables (e.g., Hermite polynomials for Gaussian random variables, Legendre polynomials for uniform random variables). This is not necessary here. The proposed reduced spectral method is general from the point of view of the distribution of the random variables. The code is given only to demonstrate that the proposed method can be implemented in a simple manner. Superior numerical methods, such as an efficient eigen-solver for large sparse matrices, may be used to make the proposed method more efficient (Listing 1).

References

[1] A. Nouy, Recent developments in spectral stochastic methods for the numerical solution of stochastic partial differential equations, Arch. Comput. Methods Engrg. 16 (2009) 251–285.
[2] D.C. Charmpis, G.I. Schueeller, M.F. Pellissetti, The need for linking micromechanics of materials with stochastic finite elements: a challenge for materials science, Comput. Mater. Sci. 41 (1) (2007) 27–37.
[3] G. Stefanou, The stochastic finite element method: past, present and future, Comput. Methods Appl. Mech. Engrg. 198 (9–12) (2009) 1031–1051.
[4] E.H. Vanmarcke, Random Fields, MIT Press, Cambridge, Mass, 1983.
[5] R. Ghanem, P. Spanos, Stochastic Finite Elements: A Spectral Approach, Springer-Verlag, New York, USA, 1991.
[6] M. Kleiber, T.D. Hien, The Stochastic Finite Element Method, John Wiley, Chichester, 1992.
[7] H.G. Matthies, C.E. Brenner, C.G. Bucher, C.G. Soares, Uncertainties in probabilistic numerical analysis of structures and solids – stochastic finite elements, Struct. Safety 19 (3) (1997) 283–336.
[8] A. Papoulis, S.U. Pillai, Probability, Random Variables and Stochastic Processes, fourth ed., McGraw-Hill, Boston, USA, 2002.
[9] R. Ghanem, The nonlinear gaussian spectrum of log-normal stochastic processes and variables, J. Appl. Mech.-ASME 66 (1989) 964–973.
[10] D.B. Xiu, G.E. Karniadakis, The Wiener–Askey polynomial chaos for stochastic differential equations, SIAM J. Sci. Comput. 24 (2) (2002) 619–644.
[11] D.B. Xiu, G.E. Karniadakis, Modeling uncertainty in flow simulations via generalized polynomial chaos, J. Comput. Phys. 187 (1) (2003) 137–167.
[12] X.L. Wan, G.E. Karniadakis, Beyond Wiener–Askey expansions: handling arbitrary PDFs, J. Sci. Comput. 27 (3) (2006) 455–464.
[13] O.C. Zienkiewicz, R.L. Taylor, The Finite Element Method, fourth ed., McGraw-Hill, London, 1991.
[14] H.G. Matthies, A. Keese, Galerkin methods for linear and nonlinear elliptic stochastic partial differential equations, Comput. Methods Appl. Mech. Engrg. 194 (12–16) (2005) 1295–1331.
[15] I. Babuska, R. Tempone, G. Zouraris, Galerkin finite element approximations of stochastic elliptic partial differential equations, SIAM J. Numer. Anal. 42 (2) (2004) 800–825.
[16] I. Babuska, R. Tempone, G. Zouraris, Solving elliptic boundary value problems with uncertain coefficients by the finite element method: the stochastic formulation, Comput. Methods Appl. Mech. Engrg. 194 (12–16) (2005) 1251–1294.
[17] R.A. Horn, C.R. Johnson, Matrix Analysis, Cambridge University Press, Cambridge, UK, 1985.
[18] W.K. Liu, T. Belytschko, A. Mani, Random field finite-elements, Int. J. Numer. Methods Engrg. 23 (10) (1986) 1831–1845.
[19] F. Yamazaki, M. Shinozuka, G. Dasgupta, Neumann expansion for stochastic finite element analysis, J. Engrg. Mech.-ASCE 114 (8) (1988) 1335–1354.
[20] S. Adhikari, C.S. Manohar, Dynamic analysis of framed structures with statistical uncertainties, Int. J. Numer. Methods Engrg. 44 (8) (1999) 1157–1178.
[21] M. Grigoriu, Galerkin solution for linear stochastic algebraic equations, J. Engrg. Mech.-ASCE 132 (12) (2006) 1277–1289.
[22] G. Falsone, N. Impollonia, A new approach for the stochastic analysis of finite element modelled structures with uncertain parameters, Comput. Methods Appl. Mech. Engrg. 191 (44) (2002) 5067–5085.
[23] C.F. Li, Y.T. Feng, D.R.J. Owen, Explicit solution to the stochastic system of linear algebraic equations $(\alpha_1 A_1 + \alpha_2 A_2 + \cdots + \alpha_m A_m)x = b$, Comput. Methods Appl. Mech. Engrg. 195 (44–47) (2006) 6560–6576.
[24] Y.T. Feng, Adaptive preconditioning of linear stochastic algebraic systems of equations, Commun. Numer. Methods Engrg. 23 (11) (2007) 10231034.
[25] M. Papadrakakis, V. Papadopoulos, Robust and efficient methods for stochastic finite element analysis using Monte Carlo simulation, Comput. Methods Appl. Mech. Engrg. 134 (3-4) (1996) 325–340.
[26] X. Ma, N. Zabaras, An adaptive hierarchical sparse grid collocation algorithm for the solution of stochastic differential equations, J. Comput. Phys. 228 (8) (2009) 3084–3113.
[27] B. Ganapathysubramanian, N. Zabaras, Sparse grid collocation schemes for stochastic natural convection problems, J. Comput. Phys. 225 (1) (2007) 652–685.
[28] P.B. Nair, A.J. Keane, Stochastic reduced basis methods, AIAA J. 40 (8) (2002) 1653–1664.
[29] S.K. Sachdeva, P.B. Nair, A.J. Keane, Comparative study of projection schemes for stochastic finite element analysis, Comput. Methods Appl. Mech. Engrg. 195 (19–22) (2006) 2371–2392.
[30] S.K. Sachdeva, P.B. Nair, A.J. Keane, Hybridization of stochastic reduced basis methods with polynomial chaos expansions, Probabilist. Engrg. Mech. 21 (2) (2006) 182–192.
[31] A. Sarkar, N. Benabbou, R. Ghanem, Domain decomposition of stochastic PDEs: theoretical formulations, Int. J. Numer. Methods Engrg. 77 (5) (2009) 689–701.
[32] G. Blatman, B. Sudret, An adaptive algorithm to build up sparse polynomial chaos expansions for stochastic finite element analysis, Probabilist. Engrg. Mech. 25 (2) (2010) 183–197.
[33] A. Nouy, A generalized spectral decomposition technique to solve a class of linear stochastic partial differential equations, Comput. Methods Appl. Mech. Engrg. 196 (45-48) (2007) 4521–4537.
[34] A. Nouy, Generalized spectral decomposition method for solving stochastic finite element equations: invariant subspace problem and dedicated algorithms, Comput. Methods Appl. Mech. Engrg. 197 (51–52) (2008) 4718–4736.
[35] M. Petyt, Introduction to Finite Element Vibration Analysis, Cambridge University Press, Cambridge, UK, 1998.
[36] V. Lenaerts, G. Kerschen, J.C. Golinval, Physical interpretation of the proper orthogonal modes using the singular value decomposition, J. Sound Vib. 249 (5) (2002) 849–865.
[37] M. Khalil, S. Adhikari, A. Sarkar, Linear system identification using proper orthogonal decomposition, Mech. System Signal Process. 21 (8) (2007) 3123–3145.
[38] P. Kerfriden, P. Gosselet, S. Adhikari, S. Bordas, Bridging the proper orthogonal decomposition methods and augmented Newton–Krylov algorithms: an adaptive model order reduction for highly nonlinear mechanical problems, Comput. Methods Appl. Mech. Engrg. 200 (5–8) (2011) 850–866.
[39] J.H. Wilkinson, The Algebraic Eigenvalue Problem, Oxford University Press, Oxford, UK, 1988.
[40] U. Ozgur, Y. Alivov, C. Liu, A. Teke, M. Reshchikov, S. Dogan, V. Avrutin, S. Cho, H. Morkoc, A comprehensive review of ZNO materials and devices, J. Appl. Phys. 98 (4) (2005).
[41] Z.C. Tu, X. Hu, Elasticity and piezoelectricity of zinc oxide crystals, single layers, and possible single-walled nanotubes, Phys. Rev. B 74 (3) (2006).
[42] M. Catti, Y. Noel, R. Dovesi, Full piezoelectric tensors of Wurtzite and zinc blende zno and zns by first-principles calculations, J. Phys. Chem. Solids 64 (11) (2003) 2183–2190.
[43] R. Chowdhury, P. Rees, S. Adhikari, F. Scarpa, S. Wilks, Electronic structures of silicon doped ZNO, Phys. B: Condens. Matter 405 (8) (2010) 1980–1985.
[44] R. Chowdhury, S. Adhikari, P. Rees, Optical properties of silicon doped ZNO, Phys. B: Condens. Matter 405 (23) (2010) 4763–4767.
[45] Z. Wang, Zinc oxide nanostructures: growth, properties and applications, J. Phys.-Condens. Matter 16 (25) (2004) R829–R858.
[46] J. Hu, X.W. Liu, B.C. Pan, A study of the size-dependent elastic properties of zno nanowires and nanotubes, Nanotechnology 19 (28) (2008).
[47] Y. Qin, X. Wang, Z.L. Wang, Microfibre-nanowire hybrid structure for energy scavenging (vol 451, p. 809, 2008), Nature 457 (7227) (2009) 340.
[48] T. Thundat, Flexible approach pays off, Nature Nanotechnol. 3 (3) (2008) 133–134.
[49] E. Gerstner, Energy harvesting: rubbed the right way, Nature Phys. 4 (3) (2008) 166.
[50] S. Xu, Y. Wei, J. Liu, R. Yang, Z.L. Wang, Integrated multilayer nanogenerator fabricated using paired nanotip-to-nanowire brushes, Nano Lett. 8 (11) (2008) 4027–4032.
[51] R. Chowdhury, S. Adhikari, F. Scarpa, Elasticity and piezoelectricity of zinc oxide nanostructure, Phys. E: Low-dimensional Syst. Nanostruct. 42 (8) (2010) 2036–2040.
[52] Y. Gao, Z.L. Wang, Electrostatic potential in a bent piezoelectric nanowire. The fundamental theory of nanogenerator and nanopiezotronics, Nano Lett. 7 (8) (2007) 2499–2505.